FUT8-directed core fucosylation of N-glycans is regulated by the glycan structure and protein environment

Ana García-García[1^], Sonia Serna[2,3^], Zhang Yang[4^], Ignacio Delso[5^], Víctor Taleb[1], Thomas Hicks[5], Raik Artschwager[2,3], Sergey Y. Vakhrushev[4], Henrik Clausen[4], Jesús Angulo[5,6,7], Francisco Corzana[8], Niels C. Reichardt[2,3,9] and Ramon Hurtado-Guerrero[1,4,10*]

[1]Institute of Biocomputation and Physics of Complex Systems (BIFI), University of Zaragoza, Mariano Esquillor s/n, Campus Rio Ebro, Edificio I+D, Zaragoza 50018, Spain

[2]CIC biomaGUNE, Paseo Miramón 182, San Sebastián 20014, Spain

[3]Basque Research and Technology Alliance (BRTA), Paseo Miramón 182, San Sebastian 20850, Spain

[4]Copenhagen Center for Glycomics, Department of Cellular and Molecular Medicine, University of Copenhagen, Copenhagen DK-2200, Denmark

[5]School of Pharmacy, University of East Anglia, Norwich Research Park, Norwich, NR4 7TJ, UK

[6]Departamento de Química Orgánica, Universidad de Sevilla, 41012, Sevilla 41012, Spain

[7] Instituto de Investigaciones Químicas (CSIC-US). Avda. Américo Vespucio, 49. 41092 Seville, Spain

[8]Departamento de Química, Universidad de La Rioja, Centro de Investigación en Síntesis Química, E-26006, Logroño, Spain

[9]CIBER-BBN, Paseo Miramón 182, San Sebastian 20014, Spain

[10]Fundación ARAID, Zaragoza 50018, Spain

^These authors contributed equally: Ana García-García, Sonia Serna, Zhang Yang and Ignacio Delso

[*]To whom correspondence should be addressed: rhurtado@bifi.es

Abstract

FUT8 is an essential α-1,6-fucosyltransferase that fucosylates the innermost GlcNAc of N-glycans, a process called core fucosylation. *In vitro*, FUT8 exhibits substrate preference for the biantennary complex N-glycan oligosaccharide (G0), but the role of the underlying protein/peptide to which N-glycans are attached remains unclear. Here, we explored the FUT8 enzyme with a series of N-glycan oligosaccharides, N-glycopeptides and an Asn-linked oligosaccharide. We found that the underlying peptide plays a role in fucosylation of paucimannose (low mannose) and high mannose N-glycans but not for complex type N-glycans. Using saturation transfer difference (STD) NMR spectroscopy, we demonstrate that FUT8 recognizes all sugar units of the G0 N-glycan and most of the amino acid residues (Asn-X-Thr) that serve as recognition sequon for the oligosaccharyltransferase (OST). The largest STD signals were observed in the presence of GDP, suggesting that prior FUT8 binding to GDP-β-L-fucose (GDP-Fuc) is required for an optimal recognition of N-glycans. We applied genetic engineering of glycosylation capacities in CHO cells to evaluate FUT8 core fucosylation of high mannose and complex-type N-glycans in cells with a panel of well characterized therapeutic N-glycoproteins. This confirmed that core fucosylation mainly occurs on complex type N-glycans, although clearly only at selected glycosites. Eliminating capacity for complex-type glycosylation in cells (KO *mgat1*) revealed that glycosites with complex-type N-glycans when converted to high mannose lost the core Fuc. Interestingly, however, for erythropoietin that is uncommon among the tested glycoproteins in efficiently acquiring tetra-antennary N-glycans, two out of three N-glycosites obtained Fuc on the high mannose N-glycans. An examination of the N-glycosylation sites of several protein crystal structures indicates that core fucosylation is mostly affected by the accessibility and nature of the N-glycan and not by the nature of the underlying peptide sequence.

These data have further elucidated the different FUT8 acceptor substrate specificities both *in vitro* and *in vivo* in cells, revealing different mechanisms for promoting core fucosylation.

Keywords:

FUT8, core fucosylation, N-glycosylation, STD-NMR, enzyme kinetics, high mannose N-glycans, complex N-glycans, paucimannose type N-glycans

Introduction

N-glycan core fucosylation is a post-translational modification (PTM) that takes place in most eukaryotes except for plants and fungi[1]. This PTM is performed by a single fucosyltransferase (FUT) named FUT8[1]. FUT8 is a Golgi-resident inverting α1-6-FUT that transfers a fucose residue from GDP-Fuc to the innermost GlcNAc moiety of N-glycans to form an α1-6-linkage[1]. Core fucosylation is essential as revealed by early postnatal death with severe growth retardation, and emphysema-like changes in the lung in mice with knockout of the *fut8* gene[1]. Mutations in *FUT8* have also been found in humans leading to a rare inherited metabolic disorder known as FUT8-CDG[2], which is characterized by a severe constellation of symptoms mimicking partly the symptoms found in the *fut8* knockout in mice. Core fucosylation is also strongly linked to cancer cell invasion and metastasis[3]. FUT8 is up-regulated in a large number of cancer types[3], proposed to be due to at least to three different mechanisms: (a) regulation of the expression of programmed cell death protein 1 (PD-1)[4]; (b) alteration of antibody-dependent cellular cytotoxicity (ADCC)[5] and (c) regulation of transforming growth factor β1 receptor (TFG-β)[6], epidermal growth factor (EGF) receptor[7], α3β1 integrin[8] and E-cadherin[9]. Based on this, FUT8 is considered a promising drug target for the treatment of a large variety of cancer types.

In vitro, FUT8 prefers to fucosylate the biantennary complex N-glycan oligosaccharide (G0)[10], requiring the presence of a terminal GlcNAc moiety on the α1-3 arm of the N-glycan with structural flexibility on the α1,6 arm[11]. However, FUT8 can also fucosylate *in vitro* high mannose N-glycopeptides that lack the terminal GlcNAc moiety on the α1-3 arm. In the latter case, a peptide/protein moiety attached to the innermost GlcNAc via an N-glycosidic linkage is essential since the lack of the peptide impairs core fucosylation[12]. In addition, these findings are also supported by previous reports that

demonstrate that some glycoproteins expressed from mammalian cells are core fucosylated in high mannose N-glycans[13-14]. Presently, it has not been shown whether FUT8 recognizes the underlying peptide of the N-glycan oligosaccharide and whether this recognition favors glycosylation of complex N-glycopeptides versus complex N-glycan oligosaccharides. Furthermore, it is unknown to which extent high mannose and paucimannose type N-glycans are fucosylated *in vivo*, or why apparently certain optimal *in vitro* N-glycan (e.g. biantennary complex N-glycan) substrates are not core fucosylated *in vivo* in the context of a native protein.

FUT8 is a multidomain enzyme composed of an N-terminal coiled-coil domain, a GT-B fold catalytic domain and a SH3 domain[15]. The molecular basis of the substrate preference together with the catalytic mechanism has been recently elucidated by solving the crystal structures of FUT8 complexed to GDP and different Asn-linked oligosaccharides and G0[10, 16-17]. In the presence of GDP, FUT8 undergoes large conformational changes in several loops that contribute to the formation of the donor substrate binding site, which in turn brings the catalytic base Glu373 into the active site, a step required for catalysis. All sugar units of the G0 are recognized by FUT8, particularly A^{G0} and B^{G0} by the catalytic domain, and C^{G0}, D^{G0}, E^{G0}, F^{G0} and G^{G0} by an exosite (see Figure 1a for the nomenclature of the sugar units), which is formed by a loop connecting both the catalytic and the SH3 domains, as well as the latter domain. This exosite and mainly the SH3 domain is proposed to fine tune branch-specific acceptor affinity through both complementarity interactions and steric restrictions[10, 16-18].

To address the influence of peptides/proteins in core fucosylation of N-glycans, we report herein a multidisciplinary approach combining chemoenzymatic synthesis, enzyme kinetics, isothermal titration calorimetry (ITC), STD NMR spectroscopy, molecular dynamics (MD) simulations, and in cell experiments applying genetic engineering to

force high-mannose type N-glycosylation on recombinant glycoproteins. Our findings reveal that FUT8 only poorly glycosylates high mannose or low mannose N-glycopeptides such as paucimannose type N-glycans, both *in vitro* and *in vivo*, and that an underlying peptide is required for glycosylation of these N-glycopeptides. Importantly, however, we do identify N-glycans on erythropoietin that are efficiently core fucosylated as high mannose glycans. Although we demonstrate that FUT8 recognizes all sugar units and also the OST sequon (Asn-X-Thr) of the G0-peptide, the kinetic and thermodynamic parameters of FUT8 on G0 and G0-peptide are very similar. Furthermore, we show that FUT8 preferentially fucosylates complex N-glycans and that some N-glycosylation sites are not fucosylated in vivo because the protein substrate amino acids surrounding the innermost GlcNAc of the N-glycan likely hinder FUT8 binding.

Results and Discussion

Kinetics of FUT8 against different N-glycan and Asn-linked oligosaccharides, and N-glycopeptides

To evaluate the role of the underlying peptide in core fucosylation of N-glycans, we synthetized a series of N-glycan and Asn-linked oligosaccharides, and N-glycopeptides (see Figure 1, and Methods). From hen egg yolk, we isolated the N-linked sialylglycopeptide (SGP)[19], with the peptide sequence "KVANKT". This glycopeptide was further modified by acetic acid treatment to remove terminal sialic acids and the galactose residues by the action of β-galactosidase to produce G0-peptide. Further treatment of this glycopeptide with PNGaseF and β-N-acetylglucosaminidase produce G0, the $Man_3GlcNAc_2$ N-glycan oligosaccharide and the $Man_3GlcNAc_2$ N-glycopeptide (Figure 1a). The Asn-linked oligosaccharide, $Man_5GlcNAc_2$-Asn, was obtained by the subsequent treatment of soybean agglutinin with Pronase and β-1,2-mannosidase (Figure 1b). Hereafter, and for simplicity, the latter three compounds will be named as M3N2, M3N2-peptide and M5N2-Asn, respectively. The identity of the compounds was verified by NMR and MALDI-TOF analysis (see Supplementary Methods section and Figure S1-S4). We qualitatively determined the activity of FUT8 over the structures prepared by MALDI-TOF MS, showing that the G0-peptide was better core fucosylated than the M3N2-peptide and the M3N2 which were very poorly glycosylated under long incubation times (Figure S1-S3). Note that we previously demonstrated by MALDI-TOF MS that G0 was also a good substrate for FUT8[16]. We then determined the FUT8 kinetic parameters of these compounds, allowing the determination of k_{cat}, K_m and k_{cat}/K_m for G0 and G0-peptide (Figure 2a,b and Figure S5). Note that the kinetics parameters for GDP-Fuc were determined in the presence of a saturated concentration of G0. The K_ms for GDP-Fuc, G0 and G0-peptide were 14.56 ± 3.4, 113.1 ± 15.43 and 133.1 ± 19.99,

respectively, and the k_{cat} was ~15 min^{-1} (Figure 2a and Table 1), a value in agreement with a previous reported k_{cat} value for FUT8 (k_{cat} of 24.6 min^{-1})[20]. The transfer reaction was also ~10-fold more catalytically efficient for GDP-Fuc than that of G0. On the contrary and as expected from our MALTI-TOF analysis, FUT8 was slower against the M3N2-peptide (~3.6-fold worse initial velocity than that of G0 and the G0-peptide at 1 mM acceptor substrate; Figure 2a and Table 1), very slow against M5N2-Asn (~14-fold worse initial velocity than that of G0/G0-peptide at 1 mM acceptor substrate), and inactive against M3N2. The data could not be fitted for FUT8 against M3N2-peptide and M5N2-Asn to get reliable kinetic parameters because FUT8 was not saturated at higher concentrations of the acceptor substrates. Collectively, these data are further supported by a previous study showing that the biantennary complex N-glycan, G0-Asn, is better substrate than M3N2-Asn and M5N2-Asn[10]. In addition, a recent report also supports our findings that the kinetic parameters are very similar among G0 and G0-peptide, implying that the peptide does not influence the kinetic parameters of G0-peptide versus G0[21].

In short, while the presence of the peptide makes no difference in the kinetic parameters of FUT8 against G0 and G0-peptide, it is clear that the peptide plays a critical role in the core fucosylation of M3N2-peptide.

Thermodynamic parameters of FUT8 against the different acceptor substrates

To determine the thermodynamic parameters of FUT8 against the different N-glycan and Asn-linked oligosaccharides, and N-glycopeptides, we performed isothermal titration calorimetry (ITC) experiments. First, we determined the K_d of GDP for binding to FUT8 (K_d = 6.1 ± 1.4 μM; Table 2, Figure 2c and Figure 2d, upper panel). Then, we evaluated whether this enzyme requires prior GDP binding to binding G0. While in the absence of GDP, FUT8 showed a very poor binding to G0 (K_d = 318 ± 139 μM), this turned out to

be the opposite in the presence of GDP (K_d = 8 ± 1.3 μM; binding to G0 was ~40-fold better in the presence of GDP than in its absence; Figure 2c,d and Table 2). The poor binding of FUT8 to G0 in the absence of GDP is also supported by previous SPR data that rendered a K_d of 390 μM[22]. These data provide compelling evidence that FUT8 likely follows an ordered bi–bi kinetic mechanism. In this mechanism, which is further supported by previous crystal structures of FUT8 complexes[10, 16-17], the enzyme is in an inactive state in the apo form (open loops) and shifts to the active state (closed loops) in the presence of GDP-Fuc. This mechanism also implies an induced-fit mechanism by GDP-Fuc that has been recently proposed[10], where the sugar nucleotide would induce the closure of several loops leading to an active state conformation. The induced-fit mechanism has become a general mechanism for GTs and has been also proposed for distant GTs such as GalNAc-T2, B4GALT1 and lactose synthase[23-25].

Having established that the presence of GDP leads to a better binding of FUT8 to G0, we determined the thermodynamic parameters for the G0-peptide, M3N2, the M3N2-peptide and M5N2-Asn in the presence of an excess of GDP. As we found out for the highly similar kinetic parameters between the G0 and G0-peptide, the K_ds for G0 and G0-peptide did not show significant differences, implying that the peptide mostly in G0-peptide is not important for the overall binding. However, and contrary to the G0 versus G0-peptide parameters, FUT8 bound to the M3N2-peptide (K_d = 406 ± 159 μM) and not to M3N2 under our conditions (Table 2 and Figure S6). In fact, we could not determine a K_d for the M3N2 glycan (Table 2). This clearly suggests that the peptide mostly may play a key role in binding to M3N2-peptide and is likely behind the reason why the M3N2-peptide is a substrate for FUT8 despite its poor affinity. Furthermore, we also could not observe a binding titration profile for M5N2-Asn, likely explaining why this was one of the worst substrates for FUT8.

A detailed analysis of the thermodynamic parameters showed that the binding of the different acceptor substrates to FUT8 was largely entropy-driven (-TΔS), while the binding of GDP was favored by a gain in enthalpy (ΔH), with a reduced entropic component (Figure 2d, lower panel, and Table 2), implying distinct interaction behaviors between these molecules. The unique thermodynamic profile exhibited by the different acceptor substrates might be due to the release of a vast number of surface water molecules from FUT8 surface upon acceptor binding, promoting a favorable desolvation entropy. On the contrary, the significant reduction in GDP-Fuc donor substrate mobility upon binding to the enzyme, along with the large number of hydrogen bonds between GDP to FUT8 are largely the major factors explaining the reduction in the entropic component and the favorable enthalpy.

We conclude that although the peptide on G0-peptide does not play a significant additional role in FUT8 turnover and binding, the presence of the peptide on M3N2-peptide is key for its binding and catalysis. These differences could be attributed to G0 per se being already a good binder to FUT8, implying that the peptide might not contribute much to binding. However, M3N2 is a poor binder whose binding to FUT8 is significantly improved by the presence of the peptide, enhancing FUT8 binding and core fucosylation.

Molecular dynamics (MD) simulations and NOESY-based NMR against M3N2-peptide and M3N2

A recent report[21] hypothesized that the presence of the peptide might drive the *anti-ψ* conformation for the core-chitobiose GlcNAc moieties of the N-glycan in the free state. This conformer, which is less stable relative to the typical *syn-ψ* conformation found in solution, was previously demonstrated to be required for FUT8 recognition and

catalysis[16]. To determine the veracity of that hypothesis, we ran molecular dynamics (MD) simulations as well as NOESY-based NMR experiments to calculate experimental internuclear average distances on M3N2 and M3N2-peptide.

Simulations for both M3N2 and M3N2-peptide were produced starting either from the *syn* and the *anti* conformers of the chitobiose core. Both *anti* conformers rapidly flipped to the more energetically stable *syn* conformation, being the preferred one along the four simulations (Figure S7). Furthermore, to get experimental evidence of the proposed conformation, internuclear average distances were determined from the initial slopes of transient NOE build-curves (Figure S8). Several 2D-NOESY experiments with increasing mixing time were acquired for both M3N2 and M3N2-peptide. Signal overlapping in M3N2 spectra made impossible the integration of enough isolated signals to calculate any distance. However, in the case of M3N2-peptide it was possible to obtain build-up curves for several proton pairs, and initial growth slopes were calculated (Figure S9). Reference distances H1A-H5A and H1B-H5B were extracted from the MD simulation for greater accuracy (Figure S10), being 2.58 Å in both cases. Inter-glycosidic distances H1B-H4A and H1B-H5A were then determined using the isolated spin pair approximation giving values of 2.60 and 3.70 Å respectively, which are compatible only with a GlcNAc-β1,4-GlcNAc *syn* conformation (Figure S11), therefore demonstrating that the peptide does not induce the energetically unfavourable *anti* conformation.

STD NMR spectroscopy of FUT8 against G0-peptide, M3N2-peptide, M3N2 and the naked peptide

Having established that the peptide does not lead to the unfavourable *anti* conformation in the free state, we performed STD NMR experiments to shed lights into the role of the peptide in core fucosylation. STD NMR allows mapping the binding epitopes of ligands

in complex with large molecules. Initially, we determined that the naked peptide itself does not interact with FUT8 either in the absence or presence of GDP, implying that the peptide is likely recognized by FUT8 only in the context of an N-glycopeptide (see Methods and Figure S12). Next, we performed STD NMR on FUT8 against M3N2 and M3N2-peptide under the same conditions described above (Figure S13-S14). Again, no STD NMR signals were observed likely due to the poor affinity of these ligands to FUT8. Since we could not obtain insights from the interaction of the peptide with FUT8 using the peptide alone or M3N2-peptide, we decided to perform additional STD NMR experiments using the G0-peptide. The G0-peptide indeed clearly displayed STD signals (see below), and the STD effects for the G0-peptide were measured under increasing NMR saturation times, producing build-up curves that were used to calculate the build up rates, which were normalised with the highest value assigned a value of 100% (Figure S15).This procedure was carried out in the absence and presence of GDP to determine whether prior GDP binding to FUT8 leads to changes in G0-peptide recognition.

In STD NMR the higher the STD effect, the closer the distance of the observed proton is to the protein surface (Methods, Figure 3 and Figure S16). As the STD signals arising from protons of the $GlcNAc^{E}$ and $GlcNAc^{G}$ moieties overlapped, the analysis is based on the average of the STD effects of both residues. In the absence of GDP (Figure 3a), a moderate STD effect is observed for every sugar ring, particularly H1 and H4 in $GlcNAc^{A}$ which shows the highest saturation transfer. Remarkably all the four acetyl groups showed high STD values, especially those on $GlcNAc^{A}$ and $GlcNAc^{B}$. The peptidic moiety showed low values, along the whole fragment (KVANKT), with only significant STD signals on Asn4, the glycosylated residue. This STD NMR binding epitope map qualitatively matches to that inferred from the previously described crystallographic structure of FUT8 complexed to G0 (PDB entry 6TKV) where the whole heptasaccharide

fits into a Y-shaped groove where $GlcNAc^A$ is the most intimately recognized sugar by FUT8[16].

When the STD NMR experiment is acquired in presence of GDP (Figure 3b), a general increase of the STD effect is observed for all proton signals. This increase is particularly remarkable for sugar units A, B, C and D. Although from the crystal structure it was suggested that FUT8 recognized $GlcNAc^E$ better than $GlcNAc^G$ [16], we could not infer that from our STD NMR experiment because the STD signals for $GlcNAc^E$ and $GlcNAc^G$ overlapped in the spectra. The peptide protons also showed an increase in STD effects, especially for Asn4 and Thr6 and to a lesser extent Val2, pointing a closer interaction of the peptide with FUT8 in the presence of GDP. However, and as shown before, FUT8 did not show differences in affinity between G0 and G0-peptide, implying that the peptide did not contribute to the overall optimal binding of G0 towards FUT8 (Figure 3b). The STD effects on GDP showed a similar pattern of that found in the crystal structure of FUT8-GDP-G0 complex[16].

We then ran 0.5 μs molecular dynamics (MD) simulations on the G0-peptide and the M3N2-peptide bound to FUT8 in the presence of GDP which showed that the peptide was relatively flexible in both complexes. This might explain that after numerous crystallographic attempts to determine the structure of FUT8 complexed to GDP and G0-peptide, we could not obtain density for the peptide. The most populated hydrogen bond between the peptide moiety and the enzyme was established between the side chain of the glycosylated Asn4 and Gly217. In the G0-peptide, the sidechain of Lys5 interacts with Glu373, and in the M3N2-peptide a low-populated hydrogen bond engaging the side chain of Thr6 and Asp368 was found. Notably, this interaction could stabilize the flexible loop comprising Asp368 and Glu373, which is required for the catalysis and may explain why the peptide fragment in M3N2 enhances fucosylation (Figure S17-S18).

In short, our STD NMR measurements suggest that the two parts of the N-glycopeptide can interact with FUT8. However, the peptide showed much lower STD values indicating longer distances to the protein surface, implying that the peptide is more dynamic than the glycan as we found by our MD simulations. The presence of GDP in the complex does not dramatically change the binding epitope nor the protein surface around the N-glycan. Yet, it enhances the interactions of FUT8 with most of the sugar units and the C-terminal residues of the peptide, further supporting the differences found in K_ds for G0 in the absence and presence of GDP. Furthermore, the finding that the peptide of M3N2-peptide is clearly recognised by FUT8 provides a plausible explanation of why the peptide of the M3N2-peptide might enhance its binding to FUT8 and in turn promote core fucosylation. Interestingly, FUT8 preferably recognizes the Asn-Lys-Thr peptide sequence, which matches the sequon found for OST, a multimeric complex that transfers a preassembled oligosaccharide to selected asparagine residues within the consensus sequence Asn-X-Ser/Thr[26]. This also implies that these two very distant GTs with different structures and donor/acceptor substrates likely share the same sequon, and that FUT8 also recognizes additional amino acids beyond the previously proposed result suggesting that FUT8 might only recognize the Asn residue[21].

Core fucosylation in cells

In the past, we first examined a panel of recombinant expressed secreted N-glycoprotein therapeutics studied extensively in glycoengineered CHO cells[27]. We included an anti-rabies virus immunoglobulin IgG1 human, erythropoietin (EPO), and three lysosomal replacement enzymes, namely glucocerebrosidase (GBA), α-galactosidase (GLA), and aspartylglucosaminidase (AGA) (Figure 4). To obtain a more global perspective of core fucosylation, we also performed knockout (KO) studies of transferases targeting a key

glycosyltransferase (Mgat1) converting high-mannose to complex N-glycan, and the GlcNAc-1-phosphotransferases (GNPTAB) which are responsible for tagging the M6P to high-mannose N-glycan for lysosomal targeting (Figure 4a). We then performed site-specific analysis to monitor effects on glycosylation of the secreted purified proteins by LC-MS, and only most abundant glycan at each site is presented in Figure 4 for demonstrating the major changes between wild type (WT) and KO cells.

When expressed in CHO^{WT} cells, these N-glycoproteins carry distinct repertoires of N-glycans at select glycosites. The lysosomal enzymes have one or more complex type (mainly biantennary) N-glycans with or without core Fuc and one or more M6P-tagged high mannose glycans without core Fuc (Figure 4b). When the capacity for M6P-tagging is eliminated by the knock out of the *gnptab* (KO *gnptab*), the M6P-tagged high mannose glycans are all converted to complex type and interestingly core Fuc is found at some but not all glycosites, as previously described[27]. We then eliminated capacity for formation of complex N-glycans (KO *mgat1*) to convert all N-glycans to high mannose structures to force substrate accumulation for the FUT8 enzyme (Figure 4c). N-glycans on the lysosomal enzymes and IgG1 converted to high mannose glycans without core Fuc. However, interestingly with EPO, the N-glycans at all three glycosites acquired core Fuc to some degree with the N65 glycosite being almost exclusively core fucosylated (Table 3). The basis for the observed differences in core fucosylation of high mannose N-glycans in the lysosomal glycoproteins and EPO is currently unknown, but we note that the general processing of the N-glycans on EPO is also different and more elaborate with almost complete tetraantennary structures. Thus, we propose that EPO and its glycosites are particularly accessible substrates for the Golgi processing enzymes included FUT8. The finding that EPO is core fucosylated in high mannose N-glycans was also recently demonstrated by Wang and colleagues but not at the level of specific N-glycosites[21]. Our

results confirm that FUT8 primarily core fucosylates complex type N-glycans, but also demonstrates that core fucosylation occurs at select N-glycosites and that high mannose glycosites can rarely become core fucosylated.

The innermost amino acids around the N-glycan GlcNAc affect core fucosylation

Our findings that the complex N-glycan at Asn19^{GBA} and Asn285^{AGA} are not core fucosylated implies that other mechanisms other than the terminal sugar moieties presence of the α1,6 arm or α1,3 arm are behind core fucosylation. To explore the molecular basis of this, we inspected the crystal structures of AGA, GLA and GBA. In addition, we also inspected the human myeloperoxidase (MPO) N-glycan acceptor sites for which Asn157/Asn317/Asn563 and Asn189/Asn225 have been shown to be core fucosylated and non-core fucosylated, respectively (Figure 5). Most of these N-glycan acceptor sites are located in loops as typically expected for the location of N-glycans[28]. Most of the inspected N-glycan acceptor sites that were core fucosylated, namely Asn59/Asn146/Asn270^{GBA}, Asn157/Asn317/Asn563^{MPO} and Asn215/Asn192^{GLA}, were solvent exposed, thus allowing FUT8 access to the N-glycan and in turn core fucosylation (Figure 5). One might expect core fucosylation to occur only in the loops. However, both Asn15^{AGA} and Asn192^{GLA} are yet core fucosylated and are located in secondary structures (Figure 4 and 5). In Asn15^{AGA}, although the innermost GlcNAc OH6 was engaged in a hydrogen bond with Glu44^{AGA} from one of the monomers forming the dimer, in the other monomer, this interaction did not take place. This implies that the innermost GlcNAc OH6 would be accessible to FUT8. However, it is not entirely clear why Asn139^{GLA} is core fucosylated because the innermost GlcNAc acetamide group and OH3 were engaged by hydrogen bonds with Asp175^{GLA}. In addition, the acetamide methyl moiety was

engaged with Phe149^{GLA} by a CH-π interaction. All these interactions likely would impede core fucosylation.

All the other non-core fucosylated N-glycan acceptor sites, Asn19^{GBA}, Asn189/Asn225^{MPO} and Asn285^{AGA}, are engaged in different interactions with surrounding amino acids of the protein acceptor substrates. The innermost GlcNAc moieties interact with the following residues around as follow: a) the GlcNAc moiety was engaged in a CH-π interaction with Tyr22^{GBA} and Trp369^{MPO} side chains; b) the GlcNAc acetamide group established hydrogen bonds with Val199^{MPO} backbone, and Gln201^{MPO} and Thr287^{AGA} side chains; and c) the GlcNAc OH6 was recognized by hydrogen bonds with Asp258^{AGA} and Ser227^{MPO} side chains (Figure 5). For these particular cases, it is reasonable that they cannot be core fucosylated as FUT8 access to the N-glycan acceptor sites is likely impeded. Further, non-interacting residues with the N-glycan acceptor sites, such as Ile5^{GBA}, Asn192/Leu194/Leu196/Leu373^{MPO} and Val286^{AGA}, would also likely impede core fucosylation due to steric clashes with FUT8.

Finally, we performed extensive MD simulations on the N-glycans of MPO, GLA, GBA and EPO present in the crystal structures (see Methods). Note that for EPO, Asn24, Asn38 and Asn83 from the crystal structure correspond to Asn51, Asn65 and Asn110 in the full-length protein, respectively. In addition, in the case of the EPO protein, three Lys residues from the crystal structure (Lys24, Lys38 and Lys83), that corresponded to Asn residues in the wild type protein, were mutated to Asn and a GlcNAc moiety was manually appended in order to understand how the sugar moiety might affect FUT8 binding. For MPO and GBA, we did not analyze all the N-glycans because there were not sugar moieties bound to some of the Asn residues. In general, we found the GlcNAc residues most susceptible for core fucosylation are those that show the higher solvent accessible surface area (SASA). Thus, GlcNAc attached to Asn19^{GBA} provides a low SASA value,

in good agreement with its absence of core fucosylation. On the other hand, GlcNAc residues attached to Asn317^{MPO}, Asn192^{GLA}, Asn139^{GLA,} Asn24^{EPO}, Asn38^{EPO} or Asn83^{EPO} exhibit high SASA values, explaining the tendency of these residues to undergo core fucosylation. The only exception is GlcNAc at Asn215^{GLA}, which presents a low SASA value and shows a clear preference to be fucosylated (Figure S19).

We conclude that in addition to the nature of α1,3 or α1,6 arm of the N-glycan that core fucosylation is also modulated by the environment of the N-glycan surrounding amino acids of the protein acceptor substrate. In particular, residues interacting with the innermost GlcNAc (e.g. the sugar moiety itself or specific positions such as the acetamide group or OH6) and non-interacting residues with the N-glycan can block FUT8 access to the N-glycan, impeding core fucosylation. This provides another avenue to regulate core fucosylation.

Conclusions

Up-regulation of core fucosylation is tightly linked to cancers and is associated with poor prognosis. This PTM may also act as a "safety switch", attenuating potentially harmful ADCC[29]. Indeed, it has been reported that 95% of IgG N-glycans in healthy individuals have core Fuc to avoid the side effect of potent ADCC due to afucosylated antibodies[29-30]. Recently, core fucosylation has been highly associated to the degree of symptoms of COVID-19, with critically ill COVID-19 patients having the highest levels of afucosylated IgG antibodies against SARS-CoV-2, leading to an increase in pro-inflammatory cytokine release and acute phase responses[31]. Due to the importance of core fucosylation in physiology and disease, it is imperative that we understand FUT8´s substrate specificity, how its activity is regulated under different conditions and how dysregulation of FUT8 relates to different pathologies.

Here, using multidisciplinary methodologies, we have inferred that two potential mechanisms are behind the acceptor substrate preferences by FUT8. In the first case, the monosaccharide residues of the α1,3/α1,6 arms determine the recognition of FUT8 on either complex N-glycans or high/low mannose N-glycans. Although this mechanism was already proposed by others, mainly at the *in vitro* level[11, 32], we postulate that FUT8 preferentially core fucosylates complex N-glycans rather than high/low mannose N-glycans *in vivo*. The second modulator of core fucosylation we believe is driven by the nature of the residues around the N-glycosylation site. In particular, residues interacting with the peptide-linked GlcNAc via the acetamide group or OH6. These hydrogen bond interactions together with additional non-interacting residues of the acceptor protein substrate would block FUT8 binding to the N-glycans, impeding core fucosylation. It was previously suggested that the more the N-glycans are exposed to the solvent, regardless of the type of N-glycan, the more likely they will be core fucosylated[21]. However, no

analysis of the N-glycans in the context of their protein acceptor substrates or MD simulations were performed. The latter calculations allowed us to obtain a more realistic scenario (exemplified by the SASA values) that reflect a more dynamic situation characterized by several conformations of the protein and the glycans, rather than only the conformation found in the crystal structure. Consequently, the absence of these data in the previous analysis may complicate the analysis of why certain and potentially favorable complex N-glycans are not core fucosylated. Although FUT8 recognizes the underlying amino acids and in particular the OST sequon, this recognition is likely not important in the overall core fucosylation process in complex N-glycans. In contrast, we found that peptide recognition is key for core fucosylation of low and high mannose N-glycans. Therefore, herein, we have thoroughly demonstrated that *in vivo* the amino acids around the N-glycan sites could play fundamental roles in modulation N-glycan core fucosylation.

In conclusion, we demonstrate that FUT8 recognizes the OST sequon but this peptide recognition is only critical for the *in vitro* core fucosylation of low and high mannose N-glycopeptides. In addition, our results confirm that FUT8 primarily core fucosylates complex type N-glycans and rarely high mannose glycosites. We also discovered that some complex N-glycan acceptor sites are not core fucosylated in cells due to surrounding amino acid residues, that may interact with the innermost GlcNAc of N-glycans or sterically clash with FUT8, implying that core fucosylation occurs at select N-glycosites. Overall, our data provide new insights into N-glycan core fucosylation *in vivo*.

Methods

Purification of FUT8

The human FUT8 was purified as previously described[12].

Isothermal titration microcalorimetry (ITC)

ITC was used to characterize the interaction of FUT8 with GDP, G0, G0-peptide, M3N2-peptide, M3N2 and M5N2-Asn. All experiments were carried out in an Auto-iTC200 (Microcal, GE Healthcare) at 25ºC. The concentration of FUT8 was 70 μM and the ligand concentration ranged from 400 μM to 1 mM. The experiments were made in 25 mM Tris pH 7.5, 150 mM NaCl for the characterization of the binding of FUT8 against GDP and G0. To characterize the binding of FUT8 against all N-glycans in the presence of an excess of GDP, the conditions were 25 mM Tris pH 7.5, 150 mM NaCl, and 1 mM GDP. The experiments were performed in duplicate. Data integration, correction and analysis were carried out in Origin 7 (Microcal). The data was fitted to a one-site equilibrium-binding model.

Kinetic analysis

Enzyme kinetics for FUT8 were determined using the GDP-Glo luminescence assays (Promega). Reactions contained 100 nM of FUT8 in 25 mM Tris pH 7.5, 150 mM NaCl and 200 μM GDP-Fucose in the presence of the ligands. The concentrations of G0, G0-peptide, M3N2-peptide, M3N2 and M5N2-Asn ranged from 5 μM to 1 mM. To determine the kinetic parameters for GDP-Fucose, we used 100 nM FUT8 in 25 mM Tris pH 7.5, 150 mM NaCl and variable concentrations of GDP-Fucose (from 5 to 500 μM) in the presence of 500 μM of G0. Reactions were incubated 30 minutes at 37 ºC and stopped using 5 μl of GDP-detection reagent at a 1:1 ratio in a white and opaque 384-well plate.

Then, the plates were incubated in the dark for 1 h at room temperature. Subsequently, the luminance values were obtained by using a Synergy HT plate reader (Biotek).

To estimate the amount of GDP produced in the glycosyltransferase reaction, we created a GDP standard curve. The values were corrected for enzyme hydrolysis in absence of the substrate acceptor and fit to a non-linear Michaelis-Menten in GraphPad Prism 6 software from which the K_m, k_{cat}, V_{max} along with their standard deviations were obtained. All the experiments were performed in duplicates.

Glycan and glycopeptide preparation

Glycans and glycopeptides were prepared from common scaffolds followed by enzymatic modifications as depicted in Figure 1, and described below.

To summarize, the preparation of G0, G0-peptide, M3N2 and M3N2-peptide derived from SGP isolated from egg yolk. M3N2 and M3N2-peptide began with the isolation of SGP from hen's egg yolk following a published procedure[19]. SGP was further processed to yield the G0-peptide, sialic acids were chemically removed with acetic acid and galactose residues were enzymatically released with β-galactosidase from *Aspergillus niger*[33].

SGP derived peptide isolation

Treatment of G0-peptide with PNGaseF, produced G0 and the corresponding peptide KVANKT. The peptide was purified by C18 chromatography employing a gradient from aqueous 0.1% trifluoroacetic acid (TFA) to 20 % MeOH in aqueous 0.1% TFA.

M3N2 and M3N2-peptide preparation

The G0-peptide and G0 were further enzymatically processed with β-N-acetylglucosaminidase (New England Biolabs) to remove terminal N-acetylglucosamine residues producing M3N2 and M3N2-peptide. The purification was performed by graphitized carbon chromatography employing a gradient from water to 50 % MeOH[19, 34].

M5N2-Asn preparation from soy bean agglutinin.

Soy bean agglutinin was purified by affinity chromatography from soy bean flour following previously published procedure[35]. M5N2-Asn was obtained by soy bean agglutinin digestion with Pronase from *Streptomyces griseus* (Sigma Aldrich) at 37ºC followed by purification on graphitized carbon and Sephadex LH-20. $Man_9GlcNAc_2Asn$ was digested with α-1,2-mannosidase from *Bacteroides thetaiotaomicron* (NZYtech) to produce M5N2-Asn[36]. Purification was done by graphitized carbon chromatography employing a gradient from water to 50 % MeOH.

Analysis of FUT8 substrate specificity by MALDI-TOF

Solutions of the different N-glycan structures (1 nmol) were incubated with FUT8 enzyme (18 μM) and GDP-fucose (2 nmol) in Tris 25 mM, 150 mM NaCl pH =7.5 (total volume of 10 μL) for 18h at RT. Reaction mixture was analyzed by MALDI-TOF mass spectrometry employing a solution of 2,5-dihydroxybenzoic acid (DHB, 5 mg/mL in CH_3CN:0.1% TFA, 30:70 containing 0.05% NaCl) as matrix. MALDI-TOF spectra were recorded on Ultraflextreme III time-of-flight mass spectrometer equipped with a pulsed Nd:YAG laser (355 nm) and controlled by FlexControl 3.3 software (Bruker Daltonics, Bremen , Germany). The m/z range was selected according to the mass of the sample and

the acquired spectra were processed with FlexAnalysis 3.3 software (Bruker Daltonics, Bremen, Germany).

Ligand Assignment and STD NMR Method

All experiments were performed at a temperature of 283K using a Bruker AVANCE-III 800MHz spectrometer with a 5 mm TXI triple resonance probe with z axis pulse field gradients (5mm PATXI 1H-13C/15N/D Z-GRD). The ligands, M3N2, M3N2-peptide, G0-peptide and naked peptide, had their labile protons exchanged with deuterium, by solving in D_2O and freeze-drying, 3 times, and finally solved at 5 mM in D_2O. M3N2-peptide, G0-peptide and naked peptide ^{1}H-NMR and ^{13}C-NMR signals were assigned using: ^{1}H-^{13}C HSQC (hsqcedetgp), ^{1}H-^{13}C HSQC-TOCSY (hsqcgpmlph), TOCSY (mlevph), COSY (cosygmpfqf) and HMBC (hmbcgplpndqf). 2D-NOESY experiments were measured for M3N2, M3N2-peptide, using Bruker pulse program noesygpph with mixing time (d8) of 100, 150, 200, 250, 300, 400, 600, 800, 1000 and 1500 ms. Relaxation time was set to 1 s. Fourier transform was applied to both dimensions and the corresponding horizontal traces were extracted for H1B (4.47 ppm) and H5A (3.42 ppm) in the case of M3N2-peptide. Phase and baseline were corrected for each trace, and the corresponding regions were integrated. Integral values were represented vs. mixing time and the linear initial part of each curve was adjusted to a line to calculate the corresponding slope (Figure S9a,b). Average H1A-H5A and H1B-H5B distances were calculated from the 1 μs MD simulation and used for the calculation according to equation in Figure S9c.

STD-NMR measurements

STD NMR spectra were measured for the corresponding N-glycans in the presence of 20 μM FUT8 both with and without GDP (1 mM) using Bruker pulse program stddiff.3. These experiments were performed in a buffer of 50 mM deuterated TRIS and 150 mM NaCl, pH of 7.4 in D_2O. A train of 50 ms Gaussian pulses were used at 0.2 mW applied on the F2 channel at -0.5 ppm (on resonance) and 40 ppm (off resonance) to obtain the STD spectra. To remove any unwanted XY magnetisation from the previous scan a spoil sequence of 2 trim pulses of 2.5 and 5 ms with a 40 % z-gradient applied for 3 ms at the start of the experiment. To suppress protein signals, a spinlock of 1.55W and 40ms was used (stddiff.3). To acquire build up curves for each of the systems the experiments were repeated with saturation times (D20) of 0.5, 1, 1.5, 2, 3, 4 and 5 s with recycle delays D1 set to be 2, 2.5, 3, 3.5, 4.5, 5.5 and 6.5 s respectively.

Stable expression of recombinant human IgG1, AGA, GLA and GBA in CHO cells

CHOZN GS-/- cells (Merck) were maintained in suspension cultures in serum-free media (EX-CELL CHO CD Fusion, cat. no 14365C), supplemented with 4 mM L-glutamine as previously described[37]. Expression construct containing anti rabies human IgG1[37] was used to establish stable expressing CHO clones as reported before. The entire coding sequence of human GLA, GBA and AGA was synthesized by Genewiz, USA. All reporter constructs were cloned into pCGS3 (Merck). Cells were seeded at 0.5×10^6 cells/mL in T25 flask (NUNC, Denmark) 24 h prior to transfection. 2 x 10^6 cells were transfected with 8 μg endotoxin-free plasmids using the Amaxa kit V and program U24 with Amaxa Nucleofector 2B (Lonza, Switzerland). 72 h post transfection cells were plated at 500 - 1,000 cells/well in 96-wells in 200 μl Minipool Plating Medium containing 80% EX-CELL® CHO Cloning Medium (Cat.no C6366) and 20% EX-CELL CD CHO Fusion media without glutamine for selection. Screenings of high expression clones were

performed by enzyme activity assay using medium for AGA, or Anti-hFc-HRP antibody (Merk). Selected clones were expanded in 50 mL TPP TubeSpin® shaking Bioreactors (180 rpm, 37°C and 5% CO_2).

Purification of recombinant reporter expressed in CHO cells

Culture media were centrifuged at 500xg for 20 min and filtered (0.45 μm). Purification of IgG1 and GLA, GBA and EPO were performed as reported in previous work[27, 37-38]. For AGA, 20% v/v of conditioning buffer (70 mM Tris-HCl, pH 7.0) was added to the media and loaded on column packed with Q-FastFlow Sepharose (GE Healthcare) pre-equilibrated with 5 column volume (CV) equilibration buffer (20mM Tris-HCl, 20 mM sodium acetate, 70 mM sodium chloride, pH 6.8). After washing the column with 6 CV of wash buffer (20 mM Tris-HCl, 20 mM sodium acetate, 70 mM sodium chloride, pH 6.8), the enzyme was one-step eluted with elution buffer (25 mM sodium acetate, 250 mM NaCl, pH 4.5) into a tube containing 300 mM sodium phosphate (pH 7.3). The eluates were diluted with 50% v/v of 4M $(NH_4)_2SO_4$ and further loaded on a Phenyl-Sepharose Fast Flow (high substitution) column (GE Healthcare). After washing and equilibrating the column with 5 CV of 2 M $(NH_4)_2SO_4$, 20 mM Tris-HCl, pH 7.0, the enzyme was eluted with elution buffer in gradient (2-0 M $(NH_4)_2SO_4$, 20 mM Tris-HCl, pH 7.0). 8.0).

CRISPR/Cas9 targeted KO in CHO cells

Gene targeting was carried out in CHO clones with stable expression of reporter proteins. Cells were seeded at 0.5 × 10^6 cells/mL in T25 flask (NUNC, Denmark) 24h prior to transfection, and 2x10^6 cells and 1 μg each of plasmid DNA of Cas9-GFP and gRNA were used for electroporation. 48 h after electroporation cells with GFP expression were

enriched by FACS. After culturing for 1 week cells were single cell sorted by FACS into 96-wells. KO clones with desired mutations were screened by a fast screening and selection method, i.e., Indel Detection by Amplicon Analysis (IDAA) as described[39]. Final clones were verified by Sanger sequencing. On average 2-5 clones were selected from each targeting event with frameshift mutations. The full list of CRISPR gRNA design and PCR primers used is listed elsewhere[37].

Sample preparation for N-glycopeptides site specific analysis

25 µg of purified GLA, GBA and AGA were dissolved in 50 mM ammonium bicarbonate (AmBic) buffer (pH 7.4) and further reduced with 10 mM dithiothreitol (DTT) at 60 °C for 45 minutes on shaker, followed by alkylation with 20 mM iodoacetamide (IAA) at 25 °C for 30 minutes in darkness. The sample was proteolytic digested with chymotrypsin (1:40 enzyme-substrate ratio). The reaction was quenched with 1 µl TFA and the digested sample was desalted by custom-made modified StageTip colums with three layers of C18 and two layers of C8 membrane (3M Empore disks, Sigma-Aldrich). Samples were eluted with two steps of 50µl 50% methanol in 0.1% formic acid. Final sample was aliquoted in two equal parts. The first aliquote was placed into a glass insert (Agilent, U.S.A.), dried completely in SpeedVac (Eppendorf, Germany) and further re-dissolved in 50ul 0.1% formic acid (FA) and submitted for nLC-MS analysis. The second aliqout was in Eppendorf tube dried completely SpeedVac re-dissolved in 50µl 50mM AmBic buffer (pH 7.4), followed by adding 1U PNGase F per sample at 37°C for 12 hours on shaker. Sample treated with PNGase F was desalted and dried by the same methods mentioned above for the first aliqout and submitted for nLC-MS/MS analysis.

IgG N-glycan analysis by CE-LIF

Analysis of IgG1 N-glycans was also performed by capillary electrophoresis as described below[40]. Briefly, 15 µL Protein G Sepharose beads (GE Healthcare) were mixed with 200 µL conditioned medium in a 96-well plate. After washing two times with 50 mM NH_4HCO_3, 1 U PNGaseF (Roche) was added and the plate incubated for 1h at 50°C. The reaction mixture was then adjusted to 87.5% ACN and mixed with 15 µL pre-equilibrated carboxylcoated magnet beads (Thermo-Scientific). Beads were washed twice in 87.5% ACN on a 96-well magnet stand, and mixed with 6 µL 40 mM APTS in 20% acetic acid and 2 µL 1 M $NaBH_3CN$ in Tetahydrofuran and incubated for 2h at 37°C. After the labeling, excess APTS was removed by washing twice in 87.5% ACN on the glycan-absorbed magnetic beads, and the labeled N-glycans were released in 40 µL MQ water. For capillary electrophoresis analysis, 2 µL of the labeled N-glycan were mixed with 8 µL HiDi Formamide and 0.05 µL 500GS-LAS standard, and injected into a genetic analyzer equipped with 24-capillary and laser-induced fluorescence detection (LIF, Thermo Fisher 3500 × l). Data were analyzed using the GeneMapper software.

nLC-MS/MS analysis for glycan and glycopeptide analysis

An EASY-nLC 1200 LC system (Thermo Fisher Scientific) interfaced via nanoSpray Flex ion source to an Orbitrap Fusion Lumos MS (Thermo Fisher Scientific) was used for MS and MS/MS analysis. A single analytical column setup using PicoFrit Emitters (New Objectives, 75 µm inner diameter) custom packed with Reprosil-Pure-AQ C18 phase (1.9-µm particle size, 19-21 cm column length) was applied in nLC. 2µl of each sample was injected onto the column, followed by eluting with a gradient of Solvent B from 3 to 32% at 200 nL/min for 45 min (Solvent A: 100% H_2O + 0.1% (v/v) formic acid, Solvent B: 80% acetonitrile + 0.1% (v/v) formic acid). With the nominal resolution setting of 120,000, precursors of MS1 scan (m/z 350-2000) were obtained. Then HCD-

MS2 of the five most abundant multiply charged precursors in the MS1 spectrum was acquired at the nominal resolution setting of 120,000. To trigger data-dependent fragmentation events, the minimum MS1 signal threshold was 50,000. Targeted MS/MS analysis was performed by setting up a targeted MSn (tMSn) Scan Properties panel thirty targeted entries were included in the Mass List Table.

Data analysis

Glycopeptide compositional analysis was obtained from *m/z* features using in-house written SysBioWare software. For *m/z* feature recognition from full MS scans Minora Feature Detector Node of the Proteome discoverer 2.2 (ThermoFisher Scientific) was used. A list of precursor ions (*m/z*, charge and retention time) was imported as ASCII data into SysBioWare and compositional assignment within 5 ppm mass tolerance was performed. The main building blocks used for the compositional analysis were: NeuAc, Hex, HexNAc, dHex and phosphate.

For N-glycopeptide compositional analysis the most prominent peptides corresponding to each potential glycosite were determined experimentally by comparing the yield of deamidated peptides before and after PNGase F treatment and also added as a building block for the compositional assignment. The peptide sequence was determined by HCD MS/MS and the abundance level was calculated from PD 2.2. A list of potential glycan and glycopeptides for each glycosite was generated and the top 10-15 of the most abundant candidates were selected for targeted MS/MS analysis to confirm the proposed structure. Each targeted MS/MS spectrum was subjected to manual interpretation. Since the same N-glycan composition may represent isobaric structures, the listed glycan structures were made to agree with literature data. The predicted enzyme functions of the targeted genes and any useful information from the MS/MS fragments. Note, the same

N-glycan composition may represent isobaric structures, so the assignments of the listed glycan structures were made to agree with the predicted enzyme functions of the targeted genes together with fragmentation information in MS/MS spectra.

Molecular Dynamics (MD) Simulations

MD simulations were performed using AMBER 20 implemented with the ff14SB and GLYCAM06j-1 force fields. The 3D models of carbohydrate M3N2 and glycopeptides M3N2-peptide, G0-peptide were generated using GLYCAM-Web (http://glycam.org). The X-ray structure of FUT8 (PDB entry 6TKV), MPO (pdb ID: 1D2V), GLA (pdb ID: 1R46), GBA (pdb ID: 5LVX) and EPO (PDB entry 1CN4) was used to simulate these proteins. The setup for the MD simulations was like that described previously in Compañón *et. al.*[41].

ASSOCIATED CONTENT

Supporting information. This information is available free of charge on the ACS Publications website. Additional methodology, and figures (19 figures) for results and discussion are provided in Supporting Information.

AUTHOR INFORMATION

*Email for Ramon Hurtado-Guerrero: rhurtado@bifi.es

ORCID

Ramon Hurtado-Guerrero: 0000-0002-3122-9401
Niels C. Reichardt: 0000-0002-9092-7023
Francisco Corzana: 0000-0001-5597-8127
Jesús Angulo: 0000-0001-7250-5639
Iñaki Delso: 0000-0001-8355-2289
Sonia Serna: 0000-0002-2085-4412
Henrik Clausen: 0000-0002-0915-5055
Sergey Vakhrushev: 0000-0002-0418-5765
Zhang Yang: 0000-0002-4756-5813

Author Contribution

A.G.-G. and V.T. purified FUT8 and also performed enzyme kinetics and ITC experiments. S.S. and R.A. synthetized the different N-glycans and N-glycopeptides. Y.Z. performed the experiments in cells and determined the N-glycan types in each protein reporter. S.Y.V. performed site specific N-glycopeptide analysis. F.C. performed the molecular dynamics simulations. I.D. and T.H performed the NMR experiments. R.H.-G. wrote the article with mainly the contribution of H.C., I. D., J. A., F.C., S.S. and N.C.R. All authors read and approved the final manuscript.

Competing Interests

The Authors declare no competing interests.

ACKNOWLEDGMENTS

We thank ARAID, Ministerio de Ciencia e Innovación (BFU2016-75633-P and PID2019-105451GB-I00 to R.H-G. and RTI2018-099592-B-C21 to F.C.), and Gobierno de Aragón (E34_R17 and LMP58_18) with FEDER (2014-2020) funds for "Building Europe from Aragón" for financial support. A.G.-G. thanks Gobierno de Aragón for a predoctoral fellowship. This work was supported by the Lundbeck Foundation, Novo Nordisk Foundation, Innovation Fund Denmark, and the Danish National Research Foundation (DNRF107). J.A. thanks funding from the Biotechnology and biological Sciences Research Council (BBSRC) through a New Investigator grant, and from the Spanish Ministry of Science, Innovation and Universities through the PID2019-109395GB-I00 project. I.D. thanks European Commission for a MSCA-IF-EF-ST grant (PyroSul, ID 890779). T.H. is supported by the UKRI Biotechnology and Biological Sciences Research Council Norwich Research Park Biosciences Doctoral Training Partnership Grant BB/M011216/1. We thank Prof. Thomas Gerken from Case Western Reserve University for proofreading the manuscript.

REFERENCES

1. Wang, X.; Inoue, S.; Gu, J.; Miyoshi, E.; Noda, K.; Li, W.; Mizuno-Horikawa, Y.; Nakano, M.; Asahi, M.; Takahashi, M.; Uozumi, N.; Ihara, S.; Lee, S. H.; Ikeda, Y.; Yamaguchi, Y.; Aze, Y.; Tomiyama, Y.; Fujii, J.; Suzuki, K.; Kondo, A.; Shapiro, S. D.; Lopez-Otin, C.; Kuwaki, T.; Okabe, M.; Honke, K.; Taniguchi, N., Dysregulation of TGF-beta1 receptor activation leads to abnormal lung development and emphysema-like phenotype in core fucose-deficient mice. *Proc Natl Acad Sci U S A* **2005,** *102* (44), 15791-6.
2. Ng, B. G.; Dastsooz, H.; Silawi, M.; Habibzadeh, P.; Jahan, S. B.; Fard, M. A. F.; Halliday, B. J.; Raymond, K.; Ruzhnikov, M. R. Z.; Tabatabaei, Z.; Taghipour-Sheshdeh, A.; Brimble, E.; Robertson, S. P.; Faghihi, M. A.; Freeze, H. H., Expanding the molecular and clinical phenotypes of FUT8-CDG. *J Inherit Metab Dis* **2020,** *43* (4), 871-879.
3. Bastian, K.; Scott, E.; Elliott, D. J.; Munkley, J., FUT8 Alpha-(1,6)-Fucosyltransferase in Cancer. *Int J Mol Sci* **2021,** *455*.
4. Okada, M.; Chikuma, S.; Kondo, T.; Hibino, S.; Machiyama, H.; Yokosuka, T.; Nakano, M.; Yoshimura, A., Blockage of Core Fucosylation Reduces Cell-Surface Expression of PD-1 and Promotes Anti-tumor Immune Responses of T Cells. *Cell Rep* **2017,** *20* (5), 1017-1028.
5. Pereira, N. A.; Chan, K. F.; Lin, P. C.; Song, Z., The "less-is-more" in therapeutic antibodies: Afucosylated anti-cancer antibodies with enhanced antibody-dependent cellular cytotoxicity. *MAbs* **2018,** *10* (5), 693-711.
6. Tu, C. F.; Wu, M. Y.; Lin, Y. C.; Kannagi, R.; Yang, R. B., FUT8 promotes breast cancer cell invasiveness by remodeling TGF-beta receptor core fucosylation. *Breast Cancer Res* **2017,** *19* (1), 111.
7. Matsumoto, K.; Yokote, H.; Arao, T.; Maegawa, M.; Tanaka, K.; Fujita, Y.; Shimizu, C.; Hanafusa, T.; Fujiwara, Y.; Nishio, K., N-Glycan fucosylation of epidermal growth factor receptor modulates receptor activity and sensitivity to epidermal growth factor receptor tyrosine kinase inhibitor. *Cancer Sci* **2008,** *99* (8), 1611-7.
8. Zhao, Y.; Itoh, S.; Wang, X.; Isaji, T.; Miyoshi, E.; Kariya, Y.; Miyazaki, K.; Kawasaki, N.; Taniguchi, N.; Gu, J., Deletion of core fucosylation on alpha3beta1 integrin down-regulates its functions. *J Biol Chem* **2006,** *281* (50), 38343-50.
9. Hu, P.; Shi, B.; Geng, F.; Zhang, C.; Wu, W.; Wu, X. Z., E-cadherin core fucosylation regulates nuclear beta-catenin accumulation in lung cancer cells. *Glycoconj J* **2008,** *25* (9), 843-50.
10. Boruah, B. M.; Kadirvelraj, R.; Liu, L.; Ramiah, A.; Li, C.; Zong, G.; Bosman, G. P.; Yang, J. Y.; Wang, L. X.; Boons, G. J.; Wood, Z. A.; Moremen, K. W., Characterizing human alpha-1,6-fucosyltransferase (FUT8) substrate specificity and structural similarities with related fucosyltransferases. *J Biol Chem* **2020,** *295* (50), 17027-17045.
11. Calderon, A. D.; Liu, Y.; Li, X.; Wang, X.; Chen, X.; Li, L.; Wang, P. G., Substrate specificity of FUT8 and chemoenzymatic synthesis of core-fucosylated asymmetric N-glycans. *Org Biomol Chem* **2016,** *14* (17), 4027-31.
12. Yang, Q.; Zhang, R.; Cai, H.; Wang, L. X., Revisiting the substrate specificity of mammalian alpha1,6-fucosyltransferase reveals that it catalyzes core fucosylation of N-glycans lacking alpha1,3-arm GlcNAc. *J Biol Chem* **2017,** *292* (36), 14796-14803.
13. Tjondro, H. C.; Ugonotti, J.; Kawahara, R.; Chatterjee, S.; Loke, I.; Chen, S.; Soltermann, F.; Hinneburg, H.; Parker, B. L.; Venkatakrishnan, V.; Dieckmann, R.; Grant, O. C.; Bylund, J.; Rodger, A.; Woods, R. J.; Karlsson-Bengtsson, A.; Struwe, W. B.; Thaysen-Andersen, M., Hyper-truncated Asn355- and Asn391-glycans modulate the

activity of neutrophil granule myeloperoxidase. *J Biol Chem* **2021**, *296*, 10.1074/jbc.RA120.016342.
14. Balog, C. I.; Stavenhagen, K.; Fung, W. L.; Koeleman, C. A.; McDonnell, L. A.; Verhoeven, A.; Mesker, W. E.; Tollenaar, R. A.; Deelder, A. M.; Wuhrer, M., N-glycosylation of colorectal cancer tissues: a liquid chromatography and mass spectrometry-based investigation. *Mol Cell Proteomics* **2012,** *11* (9), 571-85.
15. Ihara, H.; Ikeda, Y.; Toma, S.; Wang, X.; Suzuki, T.; Gu, J.; Miyoshi, E.; Tsukihara, T.; Honke, K.; Matsumoto, A.; Nakagawa, A.; Taniguchi, N., Crystal structure of mammalian alpha1,6-fucosyltransferase, FUT8. *Glycobiology* **2007,** *17* (5), 455-66.
16. Garcia-Garcia, A.; Ceballos-Laita, L.; Serna, S.; Artschwager, R.; Reichardt, N. C.; Corzana, F.; Hurtado-Guerrero, R., Structural basis for substrate specificity and catalysis of alpha1,6-fucosyltransferase. *Nat Commun* **2020,** *11* (1), 973.
17. Jarva, M. A.; Dramicanin, M.; Lingford, J. P.; Mao, R.; John, A.; Jarman, K. E.; Grinter, R.; Goddard-Borger, E. D., Structural basis of substrate recognition and catalysis by fucosyltransferase 8. *J Biol Chem* **2020,** *295* (19), 6677-6688.
18. Tomida, S.; Takata, M.; Hirata, T.; Nagae, M.; Nakano, M.; Kizuka, Y., The SH3 domain in the fucosyltransferase FUT8 controls FUT8 activity and localization and is essential for core fucosylation. *J Biol Chem* **2020,** *295* (23), 7992-8004.
19. Sun, B.; Bao, W.; Tian, X.; Li, M.; Liu, H.; Dong, J.; Huang, W., A simplified procedure for gram-scale production of sialylglycopeptide (SGP) from egg yolks and subsequent semi-synthesis of Man3GlcNAc oxazoline. *Carbohydr Res* **2014,** *396*, 62-9.
20. Ihara, H.; Ikeda, Y.; Taniguchi, N., Reaction mechanism and substrate specificity for nucleotide sugar of mammalian alpha1,6-fucosyltransferase--a large-scale preparation and characterization of recombinant human FUT8. *Glycobiology* **2006,** *16* (4), 333-42.
21. Zhang, R.; Yang, Q.; Boruah, B. M.; Zong, G.; Li, C.; Chapla, D.; Yang, J. Y.; Moremen, K.; Wang, L. X., Appropriate aglycone modification significantly expands the glycan substrate acceptability of alpha1,6-fucosyltransferase (FUT8). *Biochem J* **2021**, *478* (8), 1571–1583.
22. Kotzler, M. P.; Blank, S.; Bantleon, F. I.; Wienke, M.; Spillner, E.; Meyer, B., Donor assists acceptor binding and catalysis of human alpha1,6-fucosyltransferase. *ACS Chem Biol* **2013,** *8* (8), 1830-40.
23. Lira-Navarrete, E.; Iglesias-Fernandez, J.; Zandberg, W. F.; Companon, I.; Kong, Y.; Corzana, F.; Pinto, B. M.; Clausen, H.; Peregrina, J. M.; Vocadlo, D. J.; Rovira, C.; Hurtado-Guerrero, R., Substrate-guided front-face reaction revealed by combined structural snapshots and metadynamics for the polypeptide N-acetylgalactosaminyltransferase 2. *Angew Chem Int Ed Engl* **2014,** *53* (31), 8206-10.
24. Ramakrishnan, B.; Boeggeman, E.; Qasba, P. K., Beta-1,4-galactosyltransferase and lactose synthase: molecular mechanical devices. *Biochem Biophys Res Commun* **2002,** *291* (5), 1113-8.
25. de Las Rivas, M.; Coelho, H.; Diniz, A.; Lira-Navarrete, E.; Companon, I.; Jimenez-Barbero, J.; Schjoldager, K. T.; Bennett, E. P.; Vakhrushev, S. Y.; Clausen, H.; Corzana, F.; Marcelo, F.; Hurtado-Guerrero, R., Structural Analysis of a GalNAc-T2 Mutant Reveals an Induced-Fit Catalytic Mechanism for GalNAc-Ts. *Chemistry* **2018,** *24* (33), 8382-8392.
26. Mohorko, E.; Glockshuber, R.; Aebi, M., Oligosaccharyltransferase: the central enzyme of N-linked protein glycosylation. *J Inherit Metab Dis* **2011,** *34* (4), 869-78.
27. Tian, W.; Ye, Z.; Wang, S.; Schulz, M. A.; Van Coillie, J.; Sun, L.; Chen, Y. H.; Narimatsu, Y.; Hansen, L.; Kristensen, C.; Mandel, U.; Bennett, E. P.; Jabbarzadeh-Tabrizi, S.; Schiffmann, R.; Shen, J. S.; Vakhrushev, S. Y.; Clausen, H.; Yang, Z., The

glycosylation design space for recombinant lysosomal replacement enzymes produced in CHO cells. *Nat Commun* **2019,** *10* (1), 1785.
28. Aebi, M., N-linked protein glycosylation in the ER. *Biochim Biophys Acta* **2013,** *1833* (11), 2430-7.
29. Shinkawa, T.; Nakamura, K.; Yamane, N.; Shoji-Hosaka, E.; Kanda, Y.; Sakurada, M.; Uchida, K.; Anazawa, H.; Satoh, M.; Yamasaki, M.; Hanai, N.; Shitara, K., The absence of fucose but not the presence of galactose or bisecting N-acetylglucosamine of human IgG1 complex-type oligosaccharides shows the critical role of enhancing antibody-dependent cellular cytotoxicity. *J Biol Chem* **2003,** *278* (5), 3466-73.
30. Shields, R. L.; Lai, J.; Keck, R.; O'Connell, L. Y.; Hong, K.; Meng, Y. G.; Weikert, S. H.; Presta, L. G., Lack of fucose on human IgG1 N-linked oligosaccharide improves binding to human Fcgamma RIII and antibody-dependent cellular toxicity. *J Biol Chem* **2002,** *277* (30), 26733-40.
31. Larsen, M. D.; de Graaf, E. L.; Sonneveld, M. E.; Plomp, H. R.; Nouta, J.; Hoepel, W.; Chen, H. J.; Linty, F.; Visser, R.; Brinkhaus, M.; Sustic, T.; de Taeye, S. W.; Bentlage, A. E. H.; Toivonen, S.; Koeleman, C. A. M.; Sainio, S.; Kootstra, N. A.; Brouwer, P. J. M.; Geyer, C. E.; Derksen, N. I. L.; Wolbink, G.; de Winther, M.; Sanders, R. W.; van Gils, M. J.; de Bruin, S.; Vlaar, A. P. J.; Amsterdam, U. M. C. C.-b. s. g.; Rispens, T.; den Dunnen, J.; Zaaijer, H. L.; Wuhrer, M.; Ellen van der Schoot, C.; Vidarsson, G., Afucosylated IgG characterizes enveloped viral responses and correlates with COVID-19 severity. *Science* **2021**, *371*, 10.1126/science.abc8378.
32. Tseng, T. H.; Lin, T. W.; Chen, C. Y.; Chen, C. H.; Lin, J. L.; Hsu, T. L.; Wong, C. H., Substrate Preference and Interplay of Fucosyltransferase 8 and N-Acetylglucosaminyltransferases. *J Am Chem Soc* **2017,** *139* (28), 9431-9434.
33. Liu, L.; Prudden, A. R.; Bosman, G. P.; Boons, G. J., Improved isolation and characterization procedure of sialylglycopeptide from egg yolk powder. *Carbohydr Res* **2017,** *452*, 122-128.
34. Hamilton, B. S.; Wilson, J. D.; Shumakovich, M. A.; Fisher, A. C.; Brooks, J. C.; Pontes, A.; Naran, R.; Heiss, C.; Gao, C.; Kardish, R.; Heimburg-Molinaro, J.; Azadi, P.; Cummings, R. D.; Merritt, J. H.; DeLisa, M. P., A library of chemically defined human N-glycans synthesized from microbial oligosaccharide precursors. *Sci Rep* **2017,** *7* (1), 15907.
35. Fasina, Y. O.; Swaisgood, H. E.; Garlich, J. D.; Classen, H. L., A semi-pilot-scale procedure for isolating and purifying soybean (Glycine max) lectin. *J Agric Food Chem* **2003,** *51* (16), 4532-8.
36. Trastoy, B.; Du, J. J.; Klontz, E. H.; Li, C.; Cifuente, J. O.; Wang, L. X.; Sundberg, E. J.; Guerin, M. E., Structural basis of mammalian high-mannose N-glycan processing by human gut Bacteroides. *Nat Commun* **2020,** *11* (1), 899.
37. Yang, Z.; Wang, S.; Halim, A.; Schulz, M. A.; Frodin, M.; Rahman, S. H.; Vester-Christensen, M. B.; Behrens, C.; Kristensen, C.; Vakhrushev, S. Y.; Bennett, E. P.; Wandall, H. H.; Clausen, H., Engineered CHO cells for production of diverse, homogeneous glycoproteins. *Nat Biotechnol* **2015,** *33* (8), 842-4.
38. Schulz, M. A.; Tian, W.; Mao, Y.; Van Coillie, J.; Sun, L.; Larsen, J. S.; Chen, Y. H.; Kristensen, C.; Vakhrushev, S. Y.; Clausen, H.; Yang, Z., Glycoengineering design options for IgG1 in CHO cells using precise gene editing. *Glycobiology* **2018,** *28* (7), 542-549.
39. Yang, Z.; Steentoft, C.; Hauge, C.; Hansen, L.; Thomsen, A. L.; Niola, F.; Vester-Christensen, M. B.; Frodin, M.; Clausen, H.; Wandall, H. H.; Bennett, E. P., Fast and

sensitive detection of indels induced by precise gene targeting. *Nucleic Acids Res* **2015,** *43* (9), e59.
40. Varadi, C.; Lew, C.; Guttman, A., Rapid magnetic bead based sample preparation for automated and high throughput N-glycan analysis of therapeutic antibodies. *Anal Chem* **2014,** *86* (12), 5682-7.
41. Companon, I.; Guerreiro, A.; Mangini, V.; Castro-Lopez, J.; Escudero-Casao, M.; Avenoza, A.; Busto, J. H.; Castillon, S.; Jimenez-Barbero, J.; Asensio, J. L.; Jimenez-Oses, G.; Boutureira, O.; Peregrina, J. M.; Hurtado-Guerrero, R.; Fiammengo, R.; Bernardes, G. J. L.; Corzana, F., Structure-Based Design of Potent Tumor-Associated Antigens: Modulation of Peptide Presentation by Single-Atom O/S or O/Se Substitutions at the Glycosidic Linkage. *J Am Chem Soc* **2019,** *141* (9), 4063-4072.

TABLE LEGENDS

Table 1. Kinetic parameters for the FUT8 glycosylation of the different N-glycan and Asn-linked oligosaccharides, and N-glycopeptides used in this study using FUT8. Note that the first row defines the kinetic parameters for the donor substrate GDP-Fuc.

	K_m (μM)	V_{max} (nmol·min^{-1}·mg^{-1})	k_{cat} (min^{-1})	k_{cat}/K_m (min^{-1}·μM^{-1})
GDP-Fuc*	14.56 ± 3.4	244.3 ± 13.1	14.17 ± 0.76	0.97
G0	113.1 ± 15.43	282.1 ± 11.72	15.62 ± 0.5	0.14
G0-peptide	133.1 ± 19.99	224.7 ± 10.68	13.03 ± 0.62	0.1
M3N2	**	**	**	**
M3N2-peptide	***	***	***	***
M5N2-Asn	***	***	***	***

*The Km of GDP-Fuc was determined in the presence of a saturating concentration of G0
**Not active
***Kinetic parameters not determined (data could not be fitted to the non-linear Michaelis-Menten equation because under our conditions, FUT8 showed a linear increase of activity versus concentration of the N-glycans)

Table 2. Thermodynamic parameters for N-glycan and Asn-linked oligosaccharides, and N-glycopeptides binding to FUT8. K_d is the dissociation constant (=1/K), and ΔG, ΔH and -TΔS are the thermodynamic parameters. Stochiometry of binding in all cases was close to ~1:1. Except for the first ITC experiment in which the K_d was determined for GDP in the presence of FUT8, the rest of the ITCs were performed with the N-glycans and N-glycopeptides in the absence or presence of GDP.

	K_d (μM)	ΔG (Kcal/mol)	ΔH (Kcal/mol)	-TΔS (Kcal/mol)	n
GDP	6.1 ± 1.4	-7.09 ± 1.65	-5.02 ± 0.4	-2.07 ± 0.48	0.60
G0 (excess GDP)	8 ± 1.3	-6.89 ± 1.11	-2.42 ± 0.15	-4.47 ± 0.72	1.2
G0 (without GDP)	318 ± 134**	-4.75 ± 2	8.35 ± 4.05	-13.1 ± 6.35	1.6
G0-peptide (excess GDP)	10 ± 4	-6.82 ± 2.6	-3.2 ± 0.56	-3.62 ± 0.99	0.84

M3N2-peptide (excess GDP)	406 ± 159**	-4.6 ± 1.8	7.7 ± 1.9	-12.3 ± 4.8	1.6
M3N2 (excess GDP)	*	*	*	*	*
M5N2-Asn (excess GDP)	*	*	*	*	*

* Not measurable under our conditions. This might be due that the binding is very weak.
** Estimated values from the fitting.

Table 3. Site-specific N-glycan analysis of EPO expressed in CHO^{WT} and $CHO^{KO:mgat1}$.

EPO N-glycosite	CHO^{WT*}	$CHO^{KO:\ Mgat1}$	
		Man5-GlcNAc2-Fuc /total[#]	Man5-GlcNAc2/total[#]
N51	Bi-antennary	0.48	0.52
N65	tetra-antennary	0.90	0.10
N110	tetra-antennary	0.67	0.33

[*] Glycans at all three sites of EPO in CHO^{WT} are exclusively core-fucosylated.
[#] total is the sum of top five glycopeptide intensity at each site by LC-MS.

FIGURE LEGENDS

Figure 1. (a) Preparation of G0, G0-peptide, M3N2 and M3N2-peptide derived from the N-linked sialylglycopeptide isolated from egg yolk. (b) Preparation of M5N2-Asn from soy bean agglutinin. The nomenclature for G0 is also depicted.

Figure 2. Enzyme kinetics and ITC experiments of FUT8 on diverse N-glycan and Asn-linked oligosaccharides, and N-glycopeptides. a) Glycosylation kinetics of FUT8 against the different acceptor substrates. b) Plot comparing the catalytic efficiency (k_{cat}/K_m) of the FUT8 against GDP, G0 and G0-peptide. Additional kinetic data are given in Table 1. Note that kinetic parameters could not be obtained for M3N2-peptide and M5N2-Asn. c) ITC data for the binding of some of the ligands to FUT8. Top: raw thermogram (thermal power versus time). Bottom: binding isotherm (normalized heats versus molar ratio). d) (upper panel) Graph depicting the K_ds of the different enzyme forms. (lower panel) Thermodynamic dissection of the interaction of the different enzyme forms with the different ligands. The binding Gibbs energy (ΔG), enthalpy (ΔH), and entropy (–TΔS) are in kcal/mol. Any negative value represents a favorable contribution to the binding, whereas a positive value represents an unfavorable contribution. * denotes estimated values from the fitting.

Figure 3. Binding epitope mapping of G0-peptide with FUT8 by STD NMR in absence (a) and presence (b) of GDP. Protein saturation was achieved by irradiation at -0.50 ppm. The coloured circles represent normalized STD-NMR intensity. Only STD responses are indicated for protons that could be accurately measured. Hollow circles indicate the sum of STD intensities of overlapping $GlcNAc^E$ and $GlcNAc^G$.

Figure 4. (a) Graphic depiction of genes involved in early steps of N-glycan synthesis and (b and c) *in vivo* core fucosylation of N-glycans by site specific analysis of purified recombinant glycoproteins (IgG1, GLA, GBA, AGA and EPO) produced in CHO^{WT} and KO of *gnptab* and *mgat1*. The most abundant glycan structure at each N-glycosite of each reporter protein produced in CHO^{WT} and engineered CHO clones are displayed. All glycan structures at each glycosite were confirmed by tandem mass spectrometry (MS/MS) analysis.

Figure 5. Close-up structures of the N-glycans of GBA, MPO, AGA and GLA. Note that MPO, AGA and GLA are dimeric structures (depicted as gray and brown colors) while GBA is monomeric (grey). Asn and residues around the N-glycans are shown as sticks with carbon atoms in grey/brown and green, respectively. Hydrogen bond interactions are shown as dotted magenta lines. Note that the residue numbering in the crystal structures for GBA, MPO and AGA do not correspond to the numbering of the full-length proteins. For AGA, Asn15 and Asn285 from the crystal structure correspond to Asn38 and Asn308 in the full-length protein, respectively. For GBA, Asn19, Asn59, Asn146 and Asn70 correspond to Asn58, Asn98, Asn185 and Asn309, respectively. For MPO, Asn157, Asn189, Asn225, Asn317 and Asn563 correspond to Asn323, Asn355, Asn391, Asn483 and Asn729, respectively.

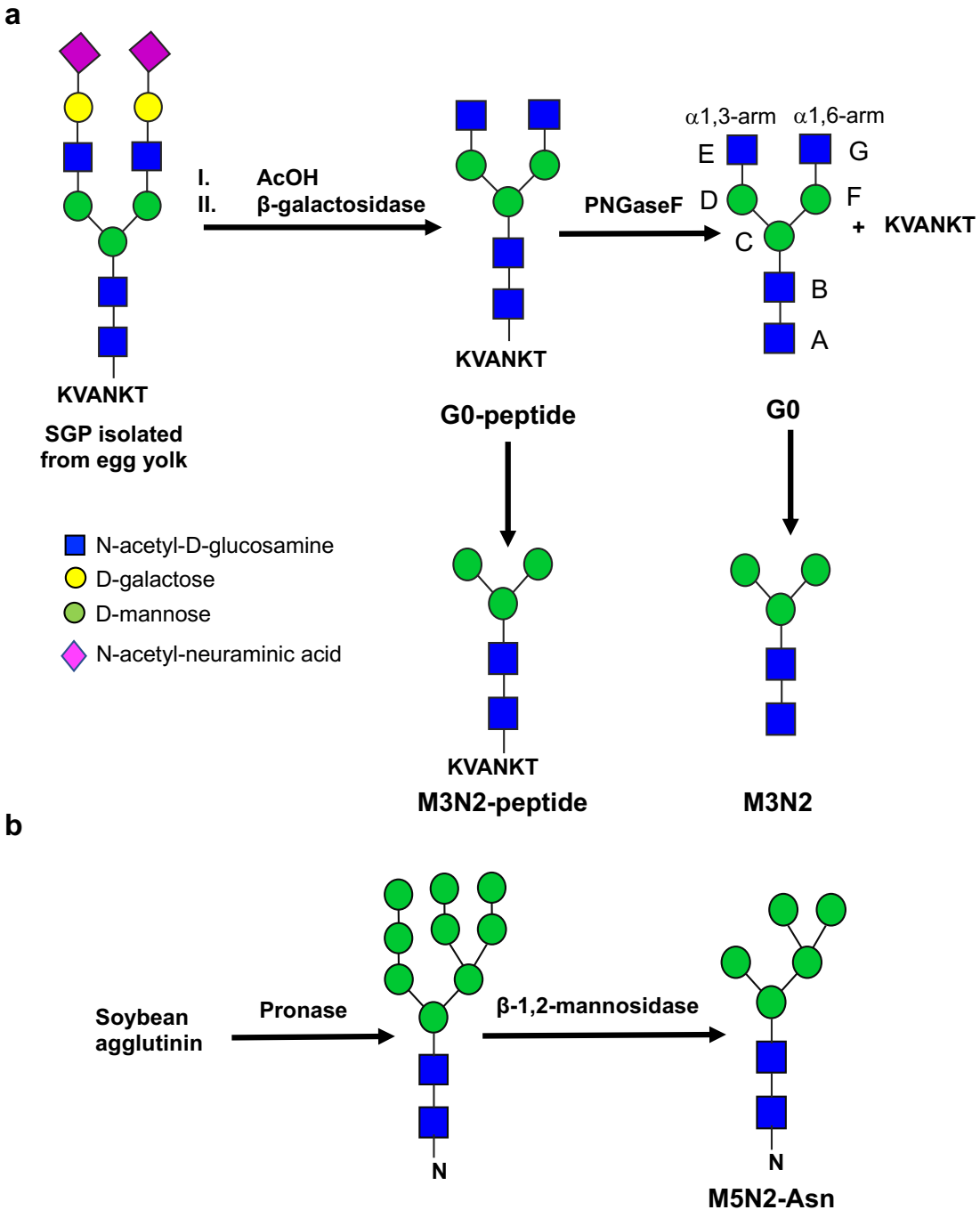

Figure 1. (a) Preparation of G0, G0-peptide, M3N2 and M3N2-peptide derived from the N-linked sialylglycopeptide isolated from egg yolk. (b) Preparation of M5N2-Asn from soy bean agglutinin. The nomenclature for G0 is also depicted.

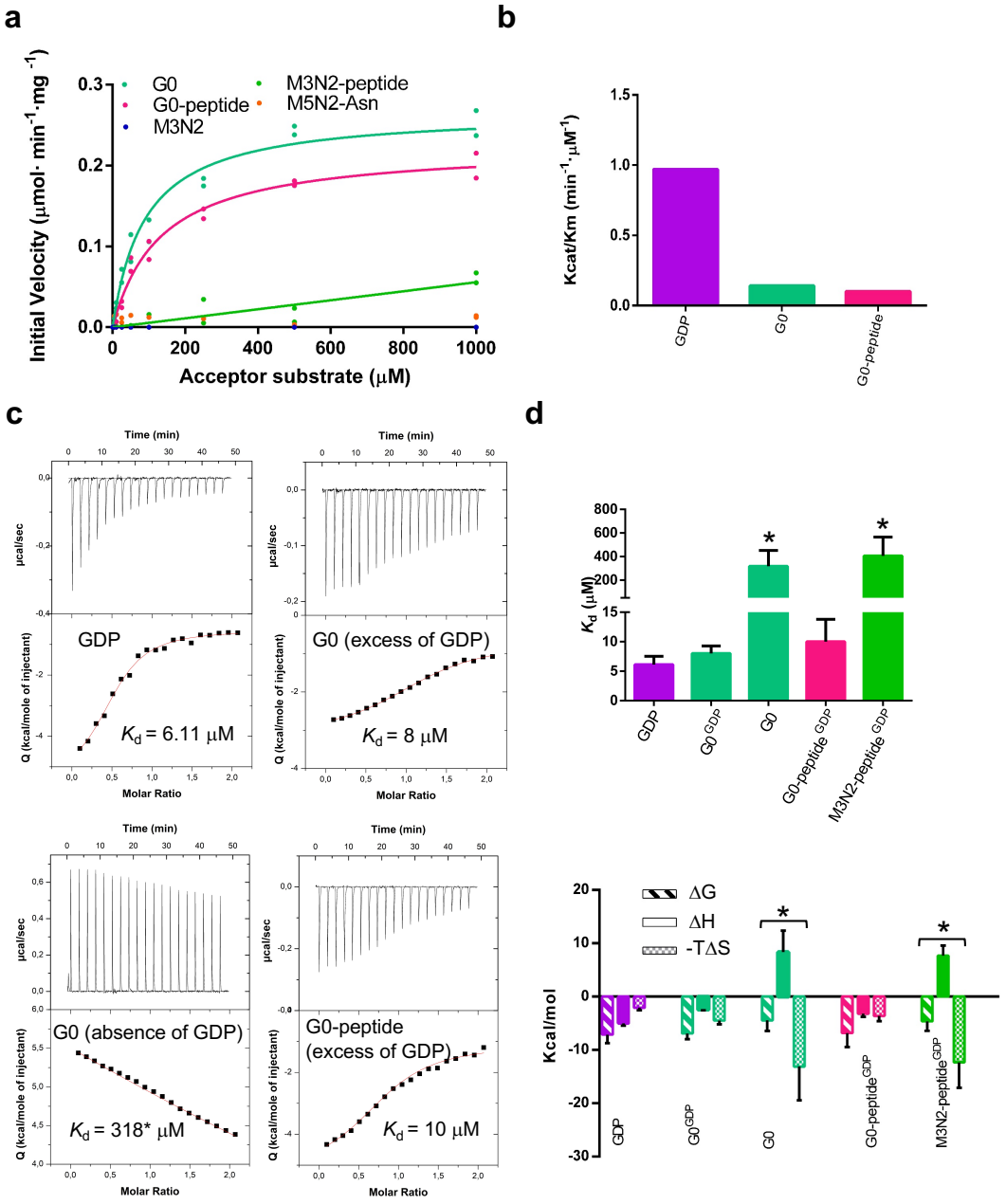

Figure 2. Enzyme kinetics and ITC experiments of FUT8 on diverse N-glycan and Asn-linked oligosaccharides, and N-glycopeptides. a) Glycosylation kinetics of FUT8 against the different acceptor substrates. b) Plot comparing the catalytic efficiency (k_{cat}/K_m) of the FUT8 against GDP, G0 and G0-peptide. Additional kinetic data are given in Table 1. Note that kinetic parameters could not be obtained for M3N2-peptide and M5N2-Asn. c) ITC data for the binding of some of the ligands to FUT8. Top: raw thermogram (thermal power versus time). Bottom: binding isotherm (normalized heats versus molar ratio). d) (upper panel) Graph depicting the K_ds of the different enzyme forms. (lower panel)

Thermodynamic dissection of the interaction of the different enzyme forms with the different ligands. The binding Gibbs energy (ΔG), enthalpy (ΔH), and entropy (–TΔS) are in kcal/mol. Any negative value represents a favorable contribution to the binding, whereas a positive value represents an unfavorable contribution.

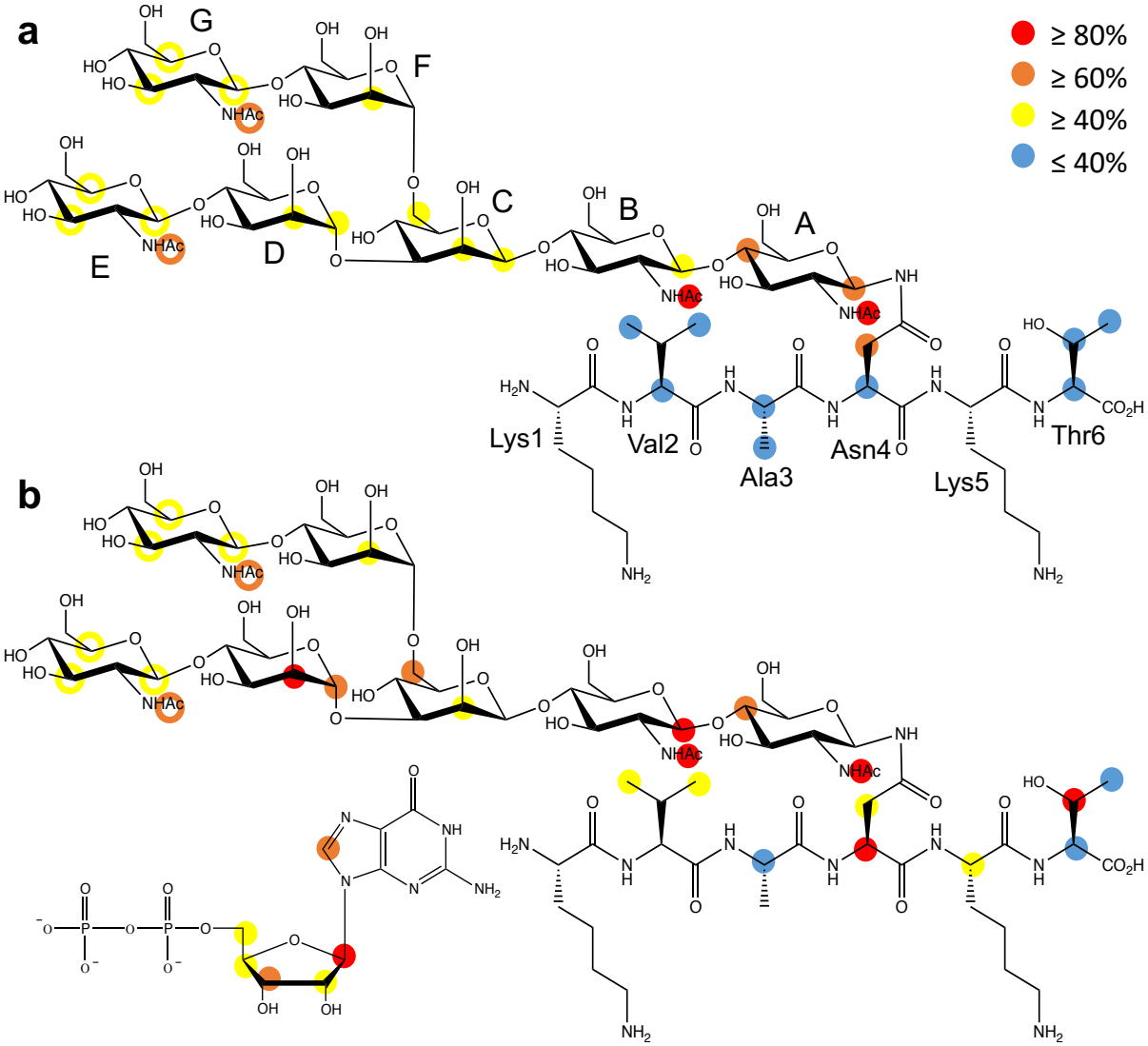

Figure 3. Binding epitope mapping of G0-peptide with FUT8 by STD NMR in absence (a) and presence (b) of GDP. Protein saturation was achieved by irradiation at -0.50 ppm. The coloured circles represent normalized STD-NMR intensity. Only STD responses are indicated for protons that could be accurately measured. Hollow circles indicate the sum of STD intensities of overlapping $GlcNAc^{E}$ and $GlcNAc^{G}$.

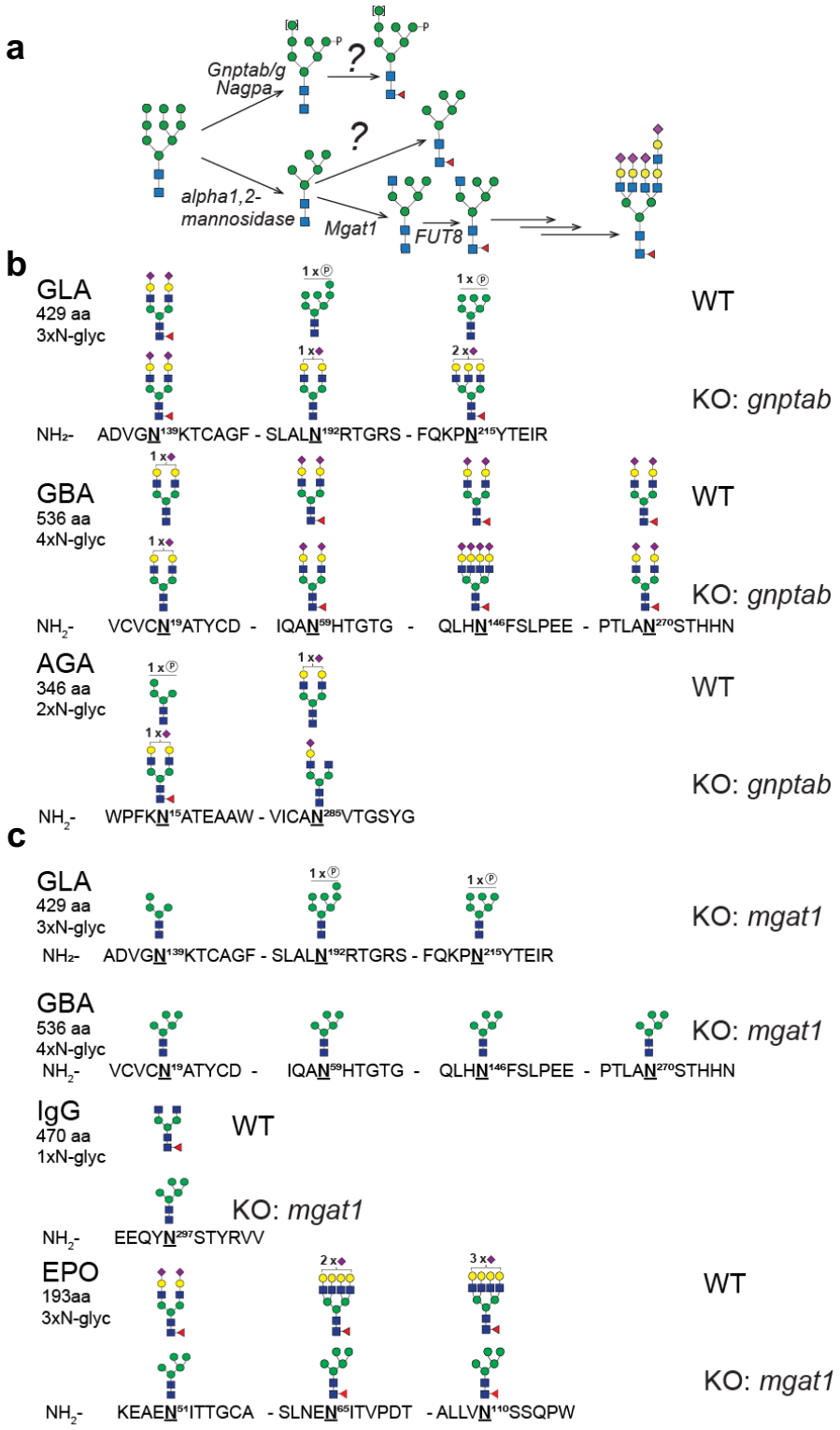

Figure 4. (a) Graphic depiction of genes involved in early steps of N-glycan synthesis and (b and c) *in vivo* core fucosylation of N-glycans by site specific analysis of purified recombinant glycoproteins (IgG1, GLA, GBA, AGA and EPO) produced in CHO^{WT} and

KO of *gnptab* and *mgat1*. The most abundant glycan structure at each N-glycosite of each reporter protein produced in CHO^{WT} and engineered CHO clones are displayed. All glycan structures at each glycosite were confirmed by tandem mass spectrometry (MS/MS) analysis.

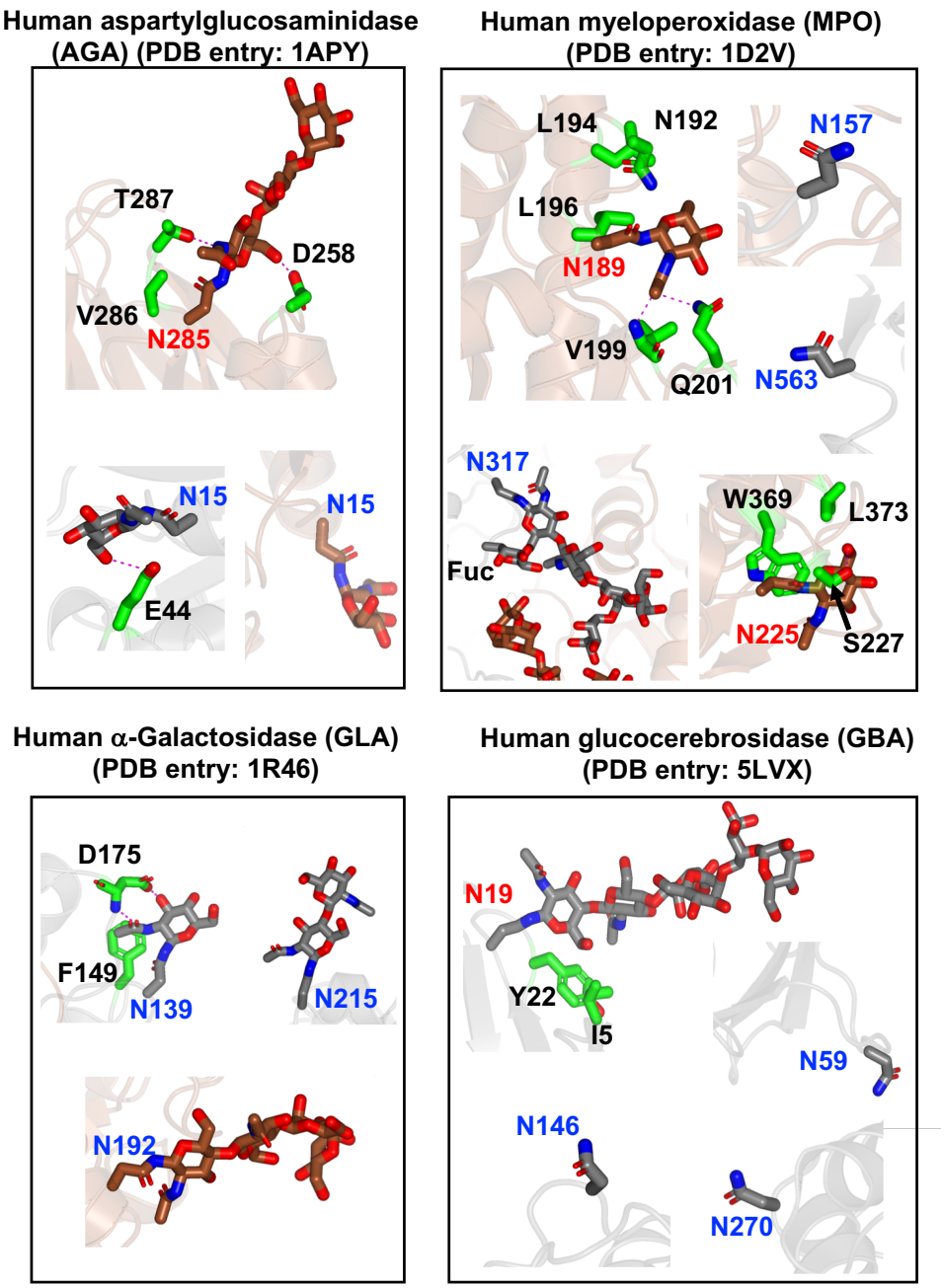

Figure 5. Close-up structures of the N-glycans of GBA, MPO, AGA and GLA. Note that MPO, AGA and GLA are dimeric structures (depicted as gray and brown colors) while GBA is monomeric (grey). Asn and residues around the N-glycans are shown as sticks with carbon atoms in grey/brown and green, respectively. Hydrogen bond interactions are shown as dotted magenta lines. Note that the residue numbering in the crystal structures for GBA, MPO and AGA do not correspond to the numbering of the full-length proteins.

For AGA, Asn15 and Asn285 from the crystal structure correspond to Asn38 and Asn308 in the full-length protein, respectively. For GBA, Asn19, Asn59, Asn146 and Asn70 correspond to Asn58, Asn98, Asn185 and Asn309, respectively. For MPO, Asn157, Asn189, Asn225, Asn317 and Asn563 correspond to Asn323, Asn355, Asn391, Asn483 and Asn729, respectively.

TOC graphic

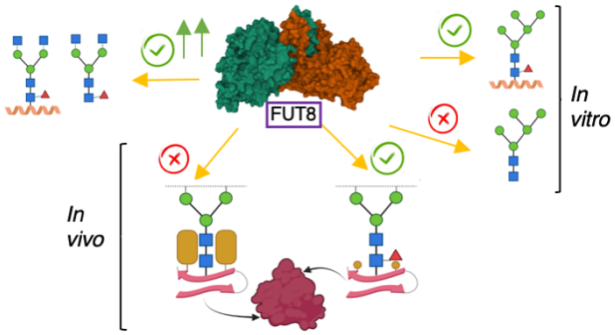

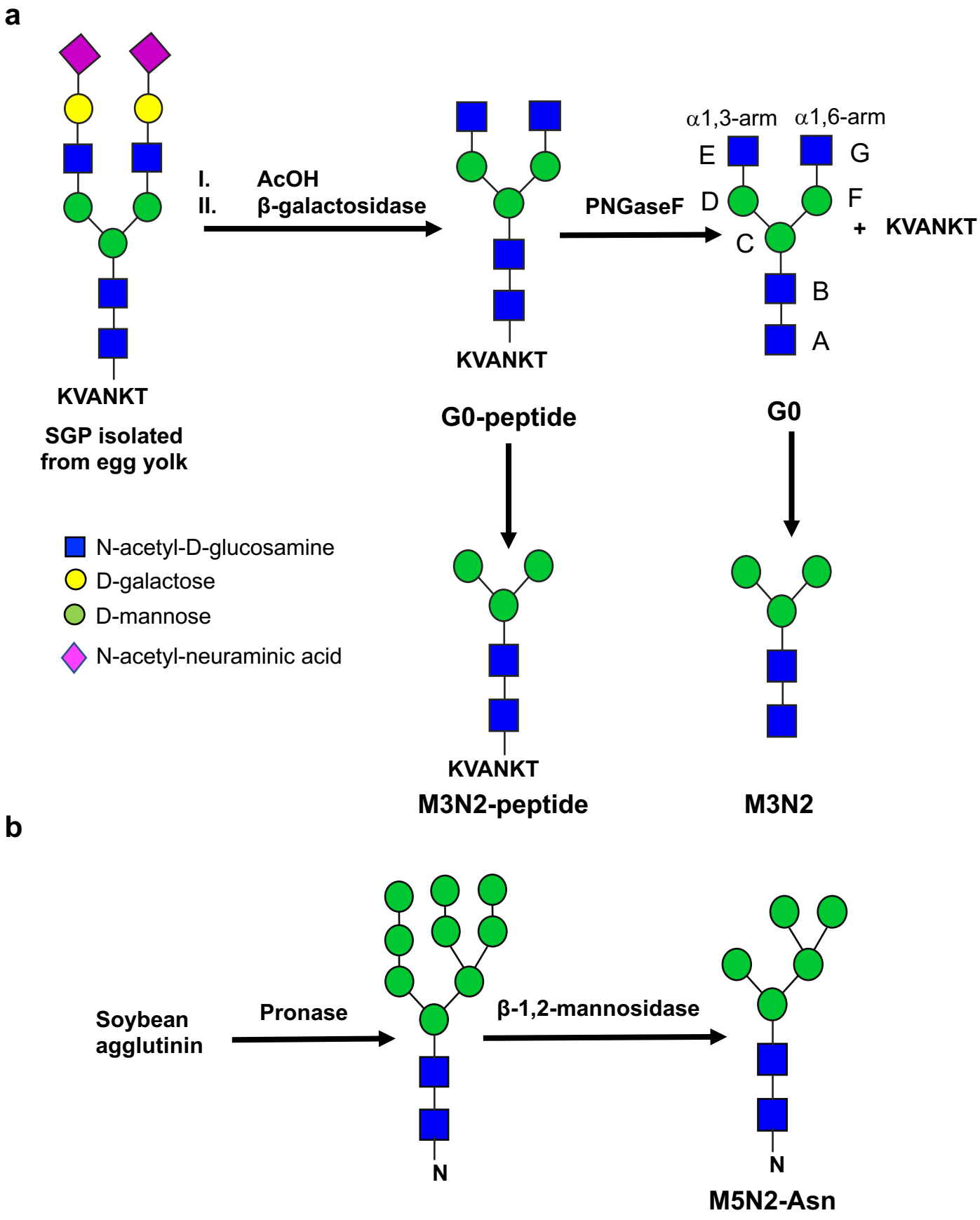
a
KVANKT
SGP isolated
from egg yolk
I. AcOH
II. β-galactosidase
KVANKT
G0-peptide
PNGaseF
α1,3-arm
α1,6-arm
E
G
D
F
C
B
A
+ KVANKT
G0
N-acetyl-D-glucosamine
D-galactose
D-mannose
N-acetyl-neuraminic acid
KVANKT
M3N2-peptide
M3N2
b
Soybean
agglutinin
Pronase
β-1,2-mannosidase
N
N
M5N2-Asn

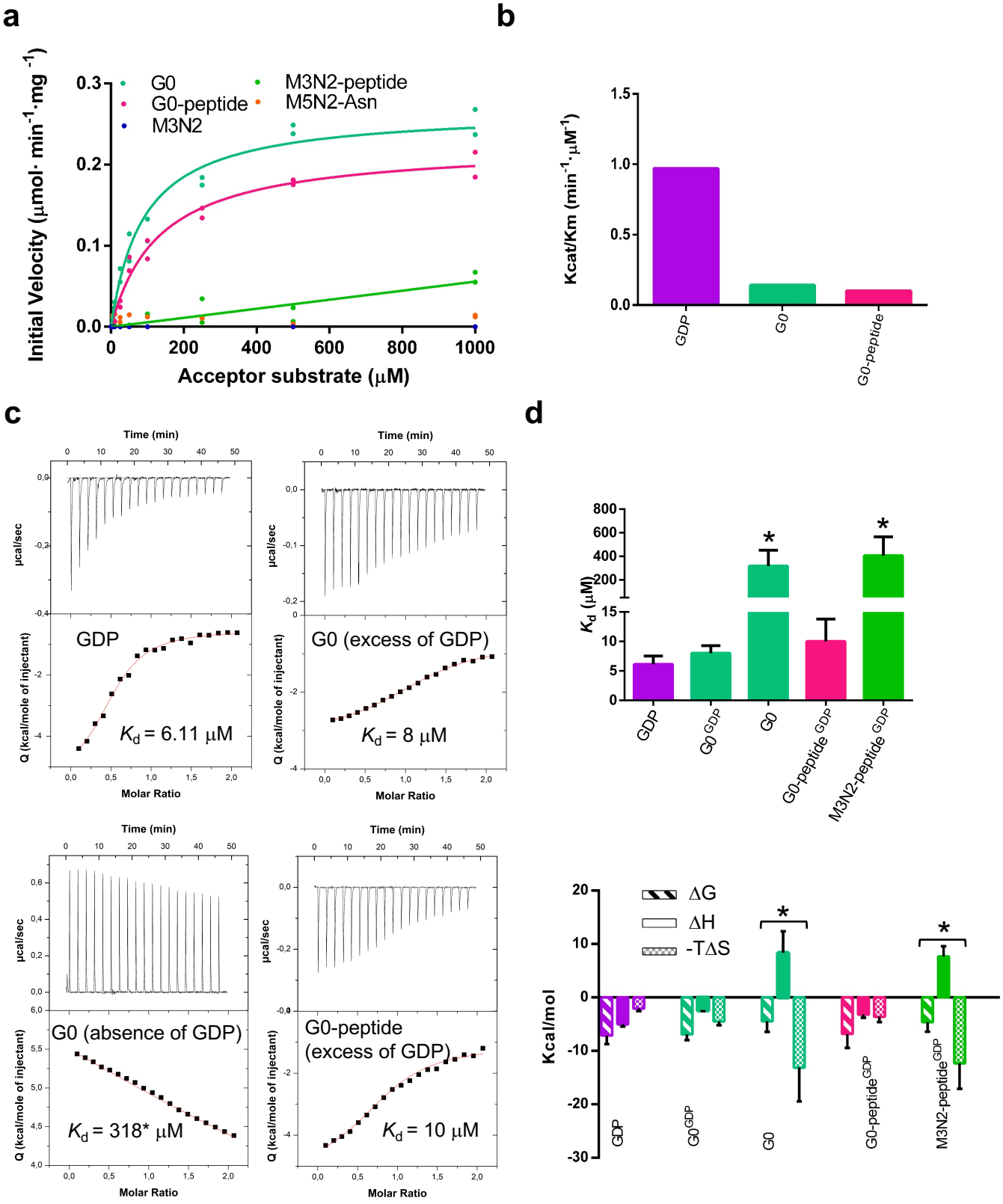
a
Initial Velocity (µmol· min-1·mg -1)
Acceptor substrate (µM)
G0
G0-peptide
M3N2
M3N2-peptide
M5N2-Asn
b
Kcat/Km (min-1·µM-1)
GDP
G0
G0-peptide
c
Time (min)
µcal/sec
Q (kcal/mole of injectant)
Molar Ratio
GDP
Kd = 6.11 µM
G0 (excess of GDP)
Kd = 8 µM
G0 (absence of GDP)
Kd = 318* µM
G0-peptide
(excess of GDP)
Kd = 10 µM
d
Kd (µM)
GDP
G0GDP
G0
G0-peptideGDP
M3N2-peptideGDP
ΔG
ΔH
-TΔS
Kcal/mol

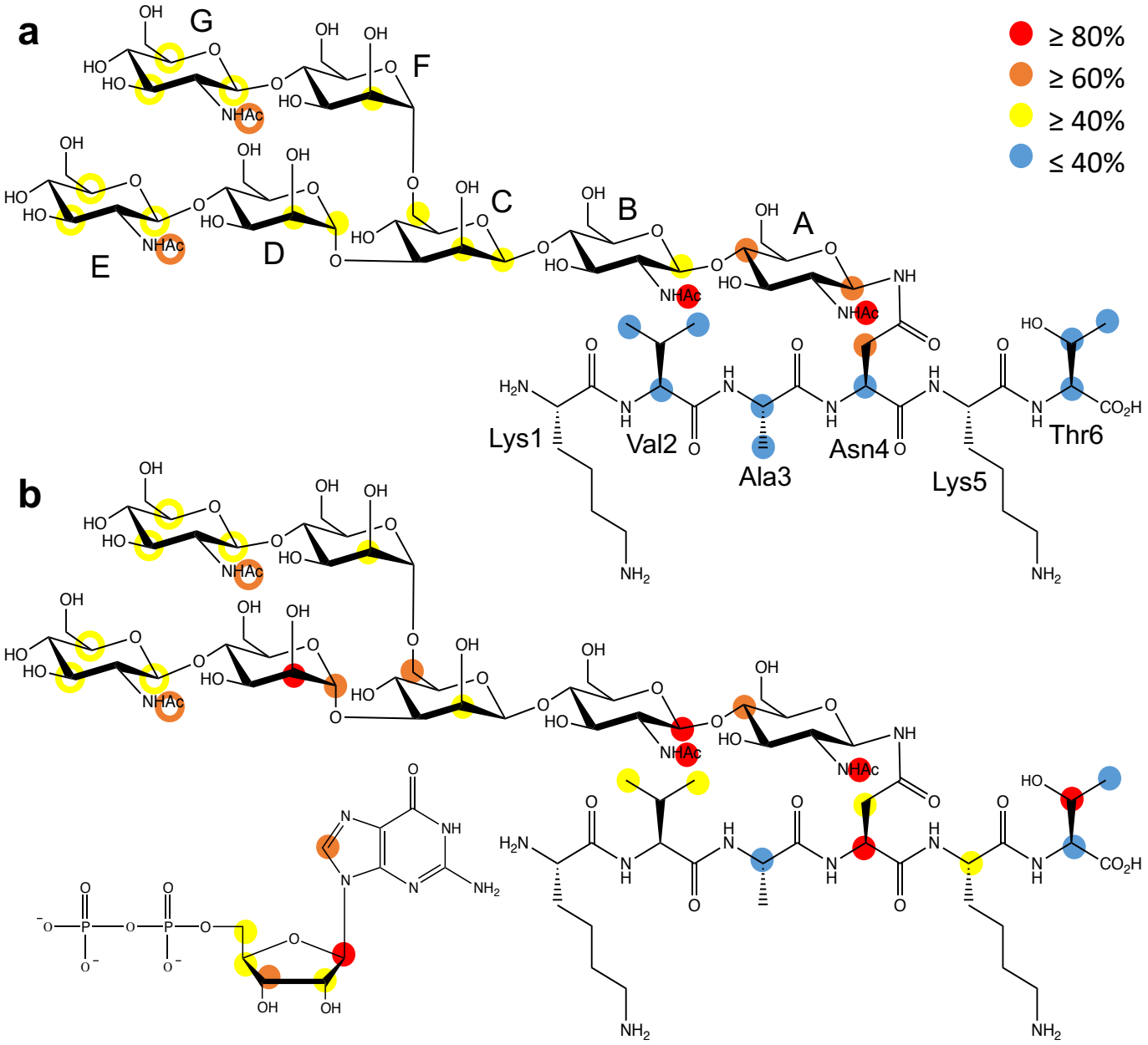
a
b
G
F
E
D
C
B
A
≥ 80%
≥ 60%
≥ 40%
≤ 40%
Lys1
Val2
Ala3
Asn4
Lys5
Thr6

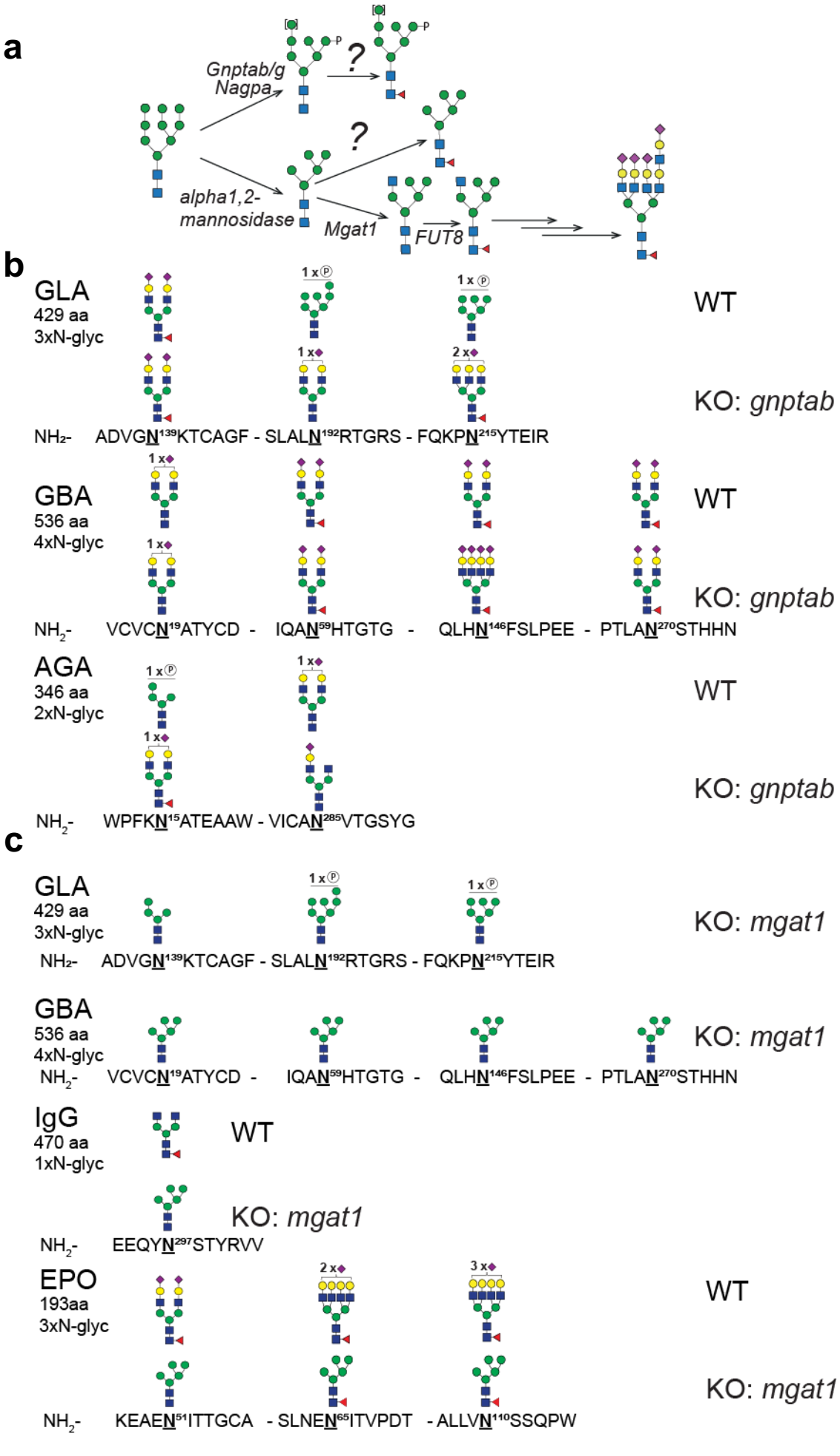
a
Gnptab/g
Nagpa
?
?
alpha1,2-
mannosidase
Mgat1
FUT8
b
GLA
429 aa
3xN-glyc
WT
KO: gnptab
NH2- ADVGN139KTCAGF - SLALN192RTGRS - FQKPN215YTEIR
GBA
536 aa
4xN-glyc
WT
KO: gnptab
NH2- VCVCN19ATYCD - IQAN59HTGTG - QLHN146FSLPEE - PTLAN270STHHN
AGA
346 aa
2xN-glyc
WT
KO: gnptab
NH2- WPFKN15ATEAAW - VICAN285VTGSYG
c
GLA
429 aa
3xN-glyc
KO: mgat1
NH2- ADVGN139KTCAGF - SLALN192RTGRS - FQKPN215YTEIR
GBA
536 aa
4xN-glyc
KO: mgat1
NH2- VCVCN19ATYCD - IQAN59HTGTG - QLHN146FSLPEE - PTLAN270STHHN
IgG
470 aa
1xN-glyc
WT
KO: mgat1
NH2- EEQYN297STYRVV
EPO
193aa
3xN-glyc
WT
KO: mgat1
NH2- KEAEN51ITTGCA - SLNEN65ITVPDT - ALLVN110SSQPW

Human aspartylglucosaminidase (AGA) (PDB entry: 1APY)

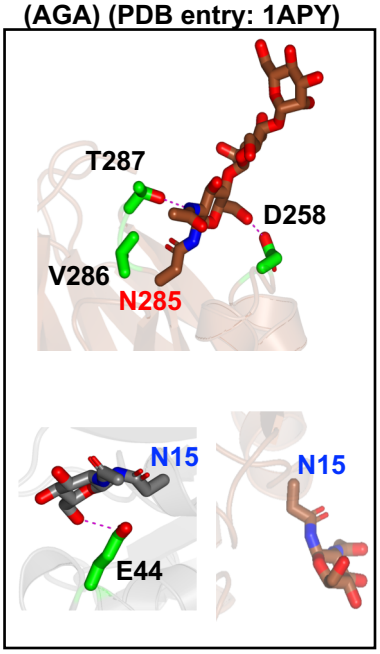

Human myeloperoxidase (MPO) (PDB entry: 1D2V)

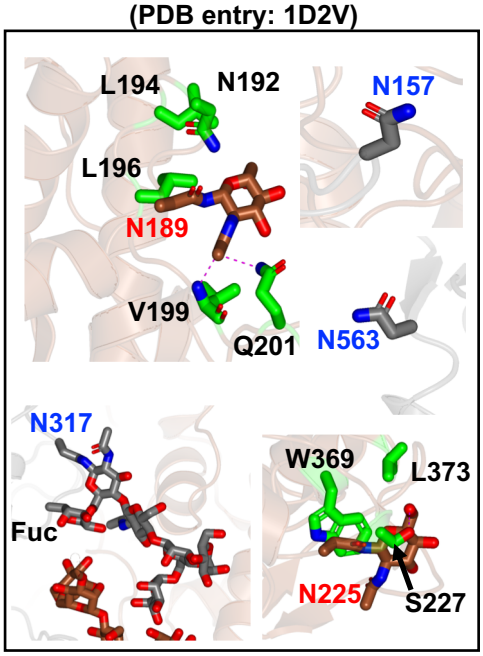

Human α-Galactosidase (GLA) (PDB entry: 1R46)

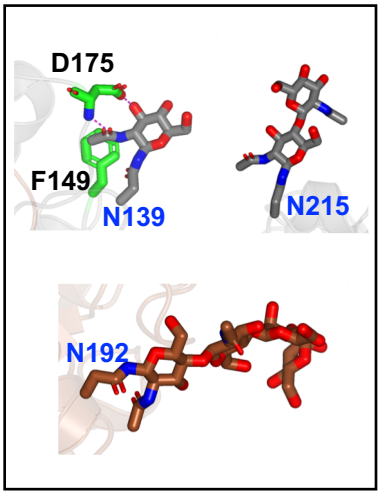

Human glucocerebrosidase (GBA) (PDB entry: 5LVX)